Annu. Rev. Nucl. Part. Sci. 2002. 52:65–113
doi: 10.1146/annurev.nucl.52.050102.090656

THE SEARCHES FOR HIGGS BOSONS AT LEP

Marumi M. Kado[1] and Christopher G. Tully[2]
[1]*Lawrence Berkeley National Laboratory, Berkeley, California 94720; e-mail: MMKado@lbl.gov;* [2]*Department of Physics, Princeton University, Princeton, New Jersey 08544; e-mail: cgtully@princeton.edu*

Key Words electroweak symmetry breaking, supersymmetry, standard model, 2HDM

PACS Codes 14.80.Bn, 12.60.Fr, 12.60.Jv

■ **Abstract** The legacy of the LEP program encompasses an extensive investigation of the electroweak interaction and the most comprehensive search to date for the origin of spontaneous symmetry breaking. The results comprise a large variety of theoretical models challenged by dedicated searches and a persistent search for the standard-model Higgs boson. The direct search for the standard-model Higgs boson confronted an excess of signal-like events in the final year. This observation reaches a significance of approximately two standard deviations for a Higgs boson mass of 115.6 GeV/c^2, a value consistent with the mass range indicated by electroweak precision measurements. The definitive confirmation of the standard-model Higgs boson search and the continued investigation for a Higgs sector at higher masses await new data from the Tevatron and LHC colliders.

CONTENTS

1. INTRODUCTION 66
1.1. The Higgs Boson 66
1.2. Experimental Situation Before the Start of LEP 69
1.3. Collider Nominal Capabilities and Detector Suitability 70
2. THE LEP1 ERA 72
2.1. Production Mechanisms 72
2.2. The Nonperturbative QCD Domain ($m_H < 2$ GeV/c^2) 72
2.3. The Perturbative QCD Domain ($2 < m_H$ up to $\sim$20 GeV/c^2) 73
2.4. Searches in the Domain $m_H < 20$ GeV/c^2 74
2.5. Searches in the Domain $m_H > 20$ GeV/c^2 74
3. THE LEP2 ERA 75
3.1. Signal Characteristics 75
3.2. Background Processes 76
3.3. Analysis Procedures 79
3.4. Search Channels and Topologies 80
3.5. Lower Limit on the Higgs Mass Before 2000 84
4. PUSHING LEP TOWARD AND BEYOND ITS LIMITS 85

4.1. Strive to Reach the Highest Energies 85
4.2. Strive to Reach the Highest Luminosities 86
4.3. Optimizing LEP for the Highest Sensitivity to the Higgs Boson 86
4.4. Synopsis of the Running of LEP in 2000 87
5. HINTS FOR THE PRODUCTION OF THE STANDARD-MODEL HIGGS BOSON AT LEP 87
5.1. Chronology 87
5.2. Mass Plots 92
5.3. Significant Events 92
5.4. Systematic Studies and Robustness of the Search 96
5.5. The ALEPH Four-Jet Events 98
6. SEARCHES FOR HIGGS BOSONS BEYOND THE STANDARD MODEL 99
6.1. Two Higgs Doublets Models (2HDM) 99
6.2. Minimal Supersymmetry 102
6.3. Beyond the Minimal Symmetric Standard Model 105
7. INDIRECT CONSTRAINTS ON THE MASS OF THE HIGGS BOSON 107
8. LEGACY AND OUTLOOK 108
9. APPENDIX: STATISTICAL METHODS 109

1. INTRODUCTION

This review is a comprehensive report on the analyses performed at CERN's Large Electron Positron Collider (LEP) to search for Higgs bosons of the standard model and beyond. It explains why searches for Higgs bosons were an important part of the LEP physics program, how these searches were performed, and what the results were. The article consists of three main sections, corresponding to the three major results of the searches for Higgs bosons at LEP:

1. the lower limit on the mass of the standard-model Higgs boson;
2. the tantalizing hints of the production of a standard-model Higgs boson with mass $m_H = 115\ \mathrm{GeV}/c^2$;
3. the close-to-exhaustive analysis of all possible Higgs boson signatures relevant to theories beyond the standard model.

Complementary to methods of data analysis were the techniques for optimizing the LEP machine performance to gain the highest sensitivity for the Higgs search. These techniques and efforts are described in detail with particular emphasis on LEP operation in the year 2000. The article concludes with a critical review of the outcome of the searches and future prospects.

1.1. The Higgs Boson

The standard model of electroweak and strong interactions at present describes all the observations remarkably well (1). Its electroweak sector relies on the gauge symmetry group $\mathrm{SU(2)_L \otimes U(1)_Y}$. The gauge invariance of the theory

requires that vector bosons be massless, which is well known not to be the case. Furthermore, the fact that this symmetry couples differently to left- and right-handed fermion fields forbids fermion mass terms, which also strongly contradicts observations.

From another standpoint, several obstacles prevent the massive intermediate vector boson theory, an extension of the Fermi model, from being a satisfactory theory of the weak interaction. On the one hand, the process $W^+W^- \to W^+W^-$ is not unitary in perturbation theory (i.e., its cross section decreases too slowly with respect to the energy), and on the other hand, the presence of massive vector bosons spoils the renormalizability of the theory.

The Higgs mechanism[1] (3), which consists of a spontaneous breaking of the electroweak symmetry, is a very elegant solution to these problems. This subtle mechanism allows gauge bosons to be massive while their interactions are still described by the $SU(2)_L \otimes U(1)_Y$ gauge group. The general concept is that the symmetry is hidden or in other words spontaneously broken, leaving the $U(1)_{EM}$ symmetry apparent to describe the electromagnetic interaction with a massless gauge boson: the photon. In this mechanism, the electroweak symmetry is spontaneously broken by the introduction of an $SU(2)_L$ doublet of scalar complex fields ϕ with the potential $V(\phi) = -\mu^2\phi^2 + \lambda\phi^4$. The spontaneous breaking occurs when the vacuum state of the scalar theory falls in a nontrivial minimum of the Higgs potential $V(\phi)$. In the fundamental state, the complex scalar doublet ϕ has a nonzero vacuum expectation value v, and the W and Z bosons acquire masses by absorbing three of the four initial degrees of freedom of the complex scalar doublet. The remaining degree of freedom is an elementary physical scalar state whose mass is not predicted at tree level by the theory: the Higgs boson. Its presence not only is a signature of the Higgs mechanism but also ensures the unitarity of the $W^+W^- \to W^+W^-$ process, as long as its mass does not exceed $\sqrt{4\pi\sqrt{2}/3G_F}$ (approximately 700 GeV). The Higgs mechanism also allows fermion masses through their Yukawa coupling to the Higgs doublet.

The Higgs mechanism is amazingly predictive. It relates the masses of the gauge bosons to the electromagnetic (e) and $SU(2)_L$ (g) coupling constants and imposes

$$\sin^2\theta_W = 1 - \frac{m_W^2}{m_Z^2} = \frac{e^2}{g^2}.$$

This tree-level prediction is verified in the present data, since the measurement of $\rho \equiv m_W^2/(m_Z^2\cos^2\theta_W)$ is found to be in very good agreement with its expected value of unity. The couplings of the Higgs boson to fermions are governed by the same Yukawa couplings that generate fermion mass terms and are thus proportional to the masses of the fermions. Therefore, the signature of the Higgs mechanism will be clear once the decay modes of the scalar boson are measured.

[1]A complete general review of the Higgs mechanism and its physical implication can be found in Reference (2).

The mass of the Higgs boson can be expressed as a function of its quartic coupling λ, the mass of the W boson, and g:

$$m_H^2 = \frac{4\lambda m_W}{g^2}.$$

Although the Higgs boson mass is a free parameter of the theory (even if the unitarity of the W^+W^- scattering imposes an upper bound), the running of the quartic coupling λ can allow us to infer both lower and upper bounds on the Higgs boson mass according to two precepts. The first is the stability of the vacuum, which requires that $\lambda > 0$ within the domain in which the theory is valid (below a given energy scale Λ above which new physics appears, superseding the standard theory) or else the Higgs potential is unstable. The second is directly inferred by the running of λ. For example, in the simple case of a pure ϕ^4 potential, the running of λ is given by

$$\frac{1}{\lambda(v)} = \frac{1}{\lambda(\Lambda)} + \frac{3}{16\pi^2}\ln\frac{\Lambda}{v},$$

which implies that

$$\lambda(v) < \frac{16\pi^2}{3\ln(\Lambda/v)} \quad \text{or} \quad m_H < \frac{4\pi v}{3\sqrt{\ln(\Lambda/v)}}.$$

This argument implies that $\lambda \to 0$ as $\Lambda \to \infty$, referred to as "triviality," and yields an upper bound on the Higgs boson mass. The bounds inferred from these two arguments are shown in Figure 1 (4). In this figure, the contribution of the top quark to the running of λ, which is essential to lead λ toward negative values, is taken into account.

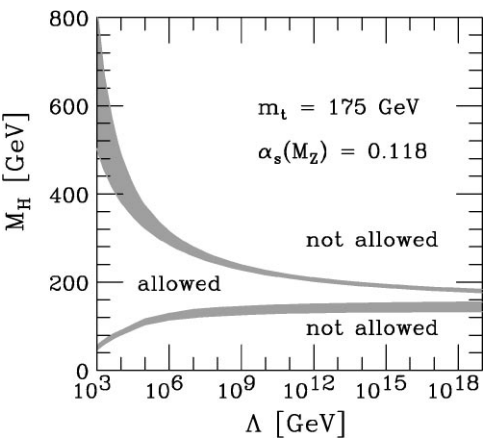

Figure 1 Lower and upper limits on the Higgs boson mass as a function of the cut-off energy scale Λ, relying on the vacuum stability and triviality arguments.

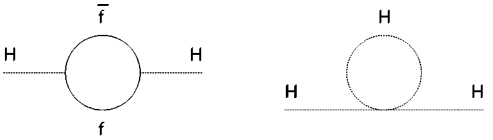

Figure 2 One-loop quadratically divergent corrections to the Higgs boson mass.

Both the arguments of unitarity and triviality tend to indicate that if the Higgs boson exists, its mass should not be exceedingly high and could thus very well be within the reach of LEP.

Although the Higgs boson resolves most of the dilemmas of the electroweak theory, it also creates a serious problem referred to as unnaturalness. Corrections to the Higgs boson mass, such as those illustrated in Figure 2, are quadratically divergent. The contribution of these loop diagrams is of the order

$$\Delta m^2 \propto \int^{\Lambda} \frac{d^4k}{(2\pi)^4} \frac{1}{k^2} \sim \frac{\Lambda^2}{16\pi^2}. \qquad 1.$$

Assuming that the cut-off (Λ) is large, typically on the Planck scale, the Higgs boson mass should naturally be of the same scale; otherwise, the bare mass would need to be fine-tuned to compensate its corrections, Δm^2 (2). We know from the unitarity and triviality arguments that the Higgs boson mass should be smaller than 1 TeV/c^2; thus, the bare mass must be fine-tuned to a precision of over 16 orders of magnitude to yield such a low value. The same problem appears at all orders of perturbation and renders the standard model very unnatural.

The standard model of electroweak interactions would work beautifully with a low-mass Higgs boson. However, if it does exist, a theory beyond the standard model is needed to solve the naturalness problem.

1.2. Experimental Situation Before the Start of LEP

Before the LEP started operation in 1989, the Higgs masses below 5 GeV/c^2 were thought to be unlikely. The uncertainty in this result comes from its reliance on the combination of numerous experiments that were subject to large theoretical uncertainties on the production cross sections and branching fractions. To illustrate some of these searches, we offer examples corresponding to the diagrams in Figure 3. For very low Higgs boson masses, the SINDRUM spectrometer experiment at the Paul Scherrer Institute (PSI) 590 MeV proton cyclotron has investigated the decay of the pion to an electron, an electron neutrino, and a Higgs boson that in turn decays to a pair of electrons (Figure 3*a*). This search resulted in an exclusion of the mass domain 10 MeV/$c^2 < m_H <$ 110 MeV/c^2 (5). The CERN-Edinburgh-Mainz-Orsay-Pisa-Siegen collaboration at the CERN Super Proton Synchrotron (SPS) also searched for the decay of a Higgs boson into a pair of electrons in the decay of $K_L^o \rightarrow \pi^o H$ (Figure 3*b*). These searches severely constrain the Higgs boson mass

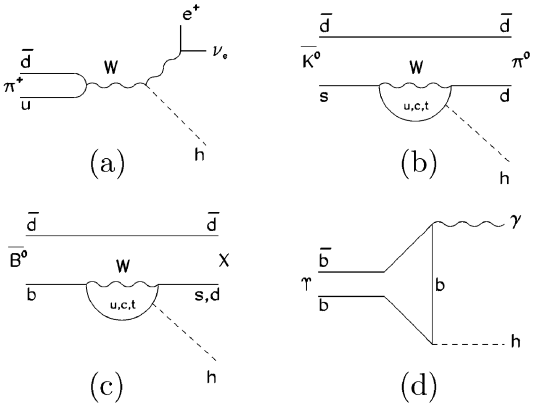

Figure 3 Light Higgs boson production via W boson or flavor-changing neutral currents.

in the domain below 50 MeV/c^2 by conferring an upper limit on the product of the branching ratios $\mathrm{Br}(K_L^o \to \pi^o H) \times \mathrm{Br}(H \to e^+e^-)$ of approximately 2×10^{-8} (6). Before 1989, the CLEO experiment investigated decays of the Higgs boson into a pair of muons, pions, and kaons produced through the flavor-changing neutral-current decay $B \to K^o H$ (Figure 3*c*). CLEO found no evidence for a Higgs boson and succeeded in excluding the mass range 0.2–3.6 GeV/c^2 (8). This exclusion relied on the evaluation of the B-to-Higgs-boson decay, which is subject to a large theoretical uncertainty. Finally, the CUSB collaboration investigated the radiative decay of various states of the Υ (7) into a Higgs boson (Figure 3*d*). The search for a monochromatic photon sample from the decay $\Upsilon \to \gamma + \mathrm{X}$ led to the exclusion of the range from $2m_\mu$ up to 5 GeV/c^2 (9). All these searches were sensitive to potentially large QCD corrections, thus justifying the importance of unambiguous searches in the low-mass region.

1.3. Collider Nominal Capabilities and Detector Suitability

1.3.1. THE LEP MACHINE The LEP collider was housed in a 26.7 km tunnel with eight 2.9-km-long arcs and eight 420-m-long straight sections. The centers of the straight sections are potential collision points. Four of them hosted LEP experiments: ALEPH, DELPHI, L3 and OPAL. Over 5000 magnets (3400 dipoles, 800 quadrupoles, 500 sextupoles, and over 600 beam orbit correctors) were installed. The effective bending radius was $\sim$3 km, although the geometric radius was about 4240 m. The first phase of operation (LEP1) extended from the summer of 1989 until 1995, when LEP operated at energies close to the Z resonance. The second phase (LEP2) started in 1995 and ended in 2000. During this time, the room-temperature (Cu) radiofrequency (RF) accelerating cavities were progressively replaced by superconducting (Nb/Cu) RF cavities able to deliver a nominal gradient

of 6 MV/m. In 2000, 288 superconducting cavities powered by 36 klystrons, supplemented by 56 Cu cavities, allowed LEP to reach a total accelerating gradient of 3630 MV/turn and a center-of-mass energy of 209 GeV.

The collider luminosity depended primarily on the beam currents and the transverse beam sizes.[2] The limiting feature for the currents was the available RF power delivered by the klystrons. Typical currents were of the order of a few mA. At LEP1, beam-beam effects limited the transverse beam sizes; this problem was overcome by the practice of running in a multiple bunch mode. From 1989 to 1992, LEP operated with four-by-four bunches (in this configuration beam crossings occur every 22 μs). To gain luminosity, from 1993 to 1995 the number of bunches was increased to eight with 11 μs spacing. In 1995, LEP proceeded to a twelve-bunch mode (four primary bunches in trains of three bunchlets 270 ns apart). As the center-of-mass energy increased, beam-beam effects decreased, and at LEP2, the running mode changed to four-by-four bunches.

Section 4 provides a more detailed description of the effort to reach the highest possible energy and luminosity at LEP2. A summary of the operation of LEP can be found in Reference (10).

1.3.2. THE DETECTORS AT LEP The four LEP detectors had similar but not identical capabilities for Higgs boson searches. The two salient features of these searches are the *b*-quark tagging and the di-jet mass determination. The di-jet mass measurements are significantly aided by energy and momentum constraints coming from knowledge of the LEP beam energy and, in most cases, the Z boson mass reconstruction.

All four LEP detectors had silicon microstrip detectors installed around the beam pipe close to the interaction region to precisely determine secondary vertices. Table 1 lists the angular coverage of the LEP detectors in terms of the cosine of the polar angle with respect to the beam. The performances of the tracking systems for momentum measurements depended on the magnetic field strength, the square of the radial dimension of the primary tracking chamber, and the position resolution in the bending plane. These parameters, listed in Table 1, indicate a range of over a factor of ten in intrinsic momentum resolutions.

The calorimeters used in the LEP detectors were separated into electromagnetic and hadronic sections; Table 2 lists the calorimeter technologies employed by the four experiments. The jet energy measurements are calibrated with Z peak data and are studied at high energy with W-mass and Z-mass measurements [from production via initial-state radiation (ISR)]. The typical, directly measured invariant mass resolution for a pair of *b*-quark jets is 8–10 GeV/c^2. Resolution effects due to the detector response and loss of energy due to semileptonic B decays can be corrected for by using kinematic constraints, such as energy-momentum conservation and the recoil to the Z boson.

For a complete description of the four detectors, see References (11–18).

[2]The luminosity also relied on the beam offsets, but these are neglected in this discussion.

TABLE 1 The four LEP detectors: the strengths of the longitudinal magnetic fields, the inner and outer radii of the primary tracking systems (the DELPHI Outer Detector is denoted OD), their position resolutions in the bending plane, and the maximum angular coverages of the silicon vertex detectors

Detector	B field (T)	r_{inner}–r_{outer} (m)	$\sigma_{r\phi}$ (μm)	$\lvert\cos\theta\rvert_{\text{max}}$
ALEPH	1.50	0.30–1.80	173	0.95
DELPHI	1.23	0.40–1.10 (TPC) 1.97–2.06 (OD)	250 110	0.91 (strips) 0.98 (pixels)
L3	0.50	0.09–0.46	50	0.93
OPAL	0.44	0.25–1.85	135	0.89

2. THE LEP1 ERA

Because of the large production cross section for a low-mass Higgs boson in Z decays, LEP provided a very good environment to further exclude small values of m_H.

2.1. Production Mechanisms

At LEP1, the Bjorken process $e^+e^- \to HZ^* \to Hf\bar{f}$, illustrated in Figure 4*a*, was assumed to be the dominant production mechanism (19). The Wilczek process (20), proceeding through a top-quark loop, $e^+e^- \to H\gamma$ (shown in Figure 4*b*) also was expected to contribute to Higgs boson production at LEP. Not only was the expected production rate through this process much smaller but backgrounds such as $e^+e^- \to q\bar{q}\gamma$ or $e^+e^- \to q\bar{q}g$, where one jet hadronizes to an energetic π^o, greatly weakened the search potential of this process. Consequently, only the Bjorken process has been extensively explored.

2.2. The Nonperturbative QCD Domain ($m_H < 2$ GeV/c^2)

For very small Higgs boson masses, such that $m_H < 2m_e$, the Higgs boson can only decay to a pair of photons via a loop of W bosons and is thus long-lived. For

TABLE 2 The calorimeter technologies of the four LEP detectors

Detector	Electromagnetic calorimeter	Hadronic calorimeter
ALEPH	Lead/wire-chamber	Iron/streamer-tube
DELPHI	Lead/projection chamber	Iron/streamer-tube
L3	BGO crystals	Uranium/gas proportional-chamber
OPAL	Lead-glass blocks	Iron/streamer-tube

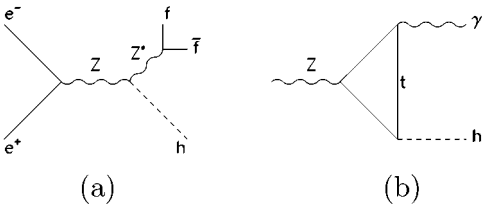

Figure 4 Higgs boson production in Z decays at LEP1: the Bjorken (*a*) and Wilczek (*b*) process.

masses below $2m_\mu$, the Higgs boson essentially decays to a pair of electrons, and below $2m_\pi$ and above $2m_\mu$ it predominantly decays to a pair of muons. Above the $2m_\pi$ threshold, the situation becomes slightly more intricate. For masses below 2–3 GeV/c^2, the Higgs boson decays to a pair of hadrons via its interaction with two gluons through a top-quark loop or its interaction with quarks. The hadronization of these gluons becomes increasingly complex at higher Higgs boson masses. Figure 5*a* depicts the branching ratios of the Higgs boson in this "nonperturbative QCD" mass range (21).

2.3. The Perturbative QCD Domain ($2 < m_H$ up to $\sim$20 GeV/c^2)

The transition to perturbative QCD is suggested by the smooth variation of the branching ratios above $\sim$2 GeV/c^2 (21, 22). Within the "perturbative QCD" domain

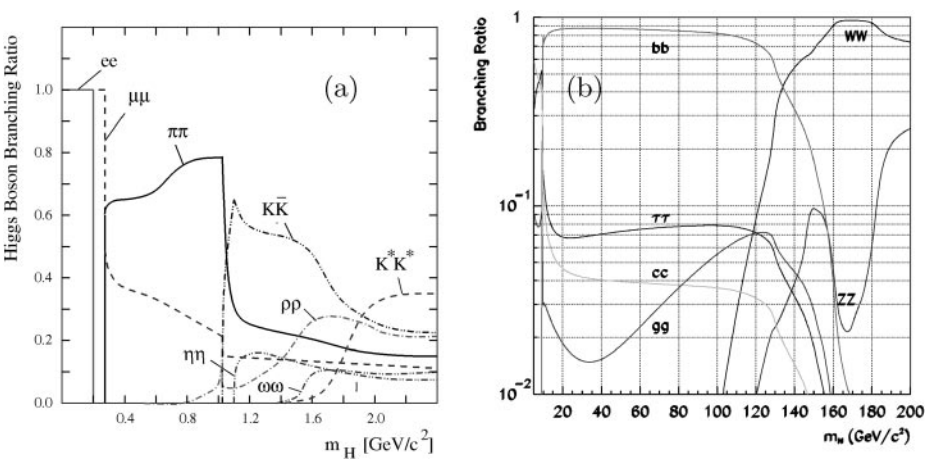

Figure 5 Higgs boson branching fractions (*a*) in the "nonperturbative QCD" low-mass range and (*b*) for heavier mass hypotheses.

and below the $b\bar{b}$ threshold, the decays into the heaviest available fermion pair ($c\bar{c}$ or $\tau^+\tau^-$) prevail because of the Higgs boson direct coupling to the fermion pair or through its coupling to a gluon pair. Above the $b\bar{b}$ threshold and for Higgs boson masses reachable at LEP (below ~ 115 GeV/c^2), the branching fractions are dominated by the decay $H \to b\bar{b}$ ($\sim$85%), as shown in Figure 5*b*.

2.4. Searches in the Domain $m_H < 20$ GeV/c^2

For a Higgs boson mass below 20 GeV/c^2, over 10,000 events were expected to be produced at LEP1 from the Higgs-strahlung process ($e^+e^- \to Z^* \to ZH$, which production cross section rapidly decreases at higher masses). Three topologies were included in the search:

1. The acoplanar lepton-pair topology, where the leptons originate from the decay of the Z. The search in this channel is essentially background-free and covers the mass domain below and around $2m_e$, where the Higgs boson is long-lived and thus escapes detection.
2. The acoplanar pair topology, where a pair of charged particles resulting from the decay of the Higgs boson recoil against a Z decaying into a pair of neutrinos.
3. The mono-jet topology, covering the hadronic decays of the Higgs boson with an intermediate mass and with a more intricate fragmentation process, where a single jet recoils against a Z^*, which decays to a pair of neutrinos.

The last two topologies, in contrast to the first, are slightly affected by the $e^+e^- \to \gamma^* Z$ background process with the Z boson decaying to a pair of neutrinos. The number of observed events in these channels was in good agreement with the standard-model background expectation. The mass domain $m_H < 20$ GeV/c^2 was therefore excluded at much more than 95% CL (23).

2.5. Searches in the Domain $m_H > 20$ GeV/c^2

In the higher Higgs boson mass domain, the Higgs boson is expected to decay dominantly to a pair of *b* quarks. The overwhelming background from the hadronic decays of the Z on the one hand and the rather small Higgs boson production rate (for $m_H = 65$ GeV/$c^2 \sim 40$ events are expected) on the other did not allow the investigation of topologies involving Z^* decays to hadrons or $\tau^\pm$. The only two channels used at LEP1 in this mass range were those where the Z^* boson decays to a pair of neutrinos or charged leptons (electrons or muons). These two topologies represent $\sim$25% of all final states. The small number of events expected (altogether ~ 10 for $m_H = 65$ GeV/c^2) to be found among the 13 million hadronic Z decays collected at LEP by all four experiments required more sophisticated analyses. In total, 13 events were observed, a number still compatible with the 20.6 events expected from the standard-model background. The results of these searches in all four experiments were combined to yield a lower limit on the Higgs boson mass of 65.6 GeV/c^2 (23–27).

3. THE LEP2 ERA

3.1. Signal Characteristics

The dominant cross sections for Higgs production at LEP2 follow from the direct coupling of the Higgs scalar to the Z and W vector bosons. This means, in particular, that the production cross sections are directly related to the Higgs mechanism for electroweak symmetry breaking and are not strongly dependent on the couplings of the Higgs field to fermions. Figure 6 shows the tree-level Feynman diagrams for the Higgs-strahlung and fusion processes (28–30). The cross sections are calculated taking into account the interference for the $H\nu_e\bar{\nu}_e$ and He^+e^- final states. Figure 7 shows the contributions to the total Higgs production cross section at a center-of-mass energy of 206.6 GeV and the total cross section at $\sqrt{s} =$ 209 GeV. These correspond, respectively, to center-of-mass energies of the highest statistical significance to the Higgs boson search and to the highest achieved LEP energy.

The kinematic threshold for Higgs boson production is clearly visible in Figure 7 where the cross section falls rapidly around $m_{\text{thres}} = \sqrt{s} - m_Z$. Above m_{thres}, the Higgs-strahlung process is still dominant because of the width of the Z, even though the relative contribution of the WW fusion increases. The reach of the LEP Higgs search, therefore, critically depended on the LEP energy and luminosity.

The Higgs branching ratios are plotted in Figure 5. The dominant branching ratio continues to be the $H \to b\bar{b}$ decay mode in the Higgs mass region accessible to production at LEP. The uncertainties in the branching ratios come primarily from uncertainty in the effective quark masses.

The standard-model Higgs boson search was performed for a set of channels, categorized by the Higgs decay and the pair of fermions either from Z decay or the fusion processes. Table 3 lists the percentages of Higgs events in the different channels for $m_H = 115\ \text{GeV}/c^2$ and $\sqrt{s} = 206.5$ GeV. The Higgs decay branching ratios for $m_H = 115\ \text{GeV}/c^2$ add up to 91.1%, with the remaining percentage primarily producing the $H \to WW^*$ decay. This decay mode, which contains a number of search channels, has an insufficient sensitivity to contribute significantly to the standard-model search at LEP.

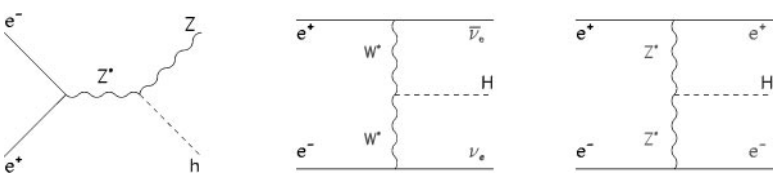

Figure 6 Diagrams of the Higgs-strahlung and the gauge boson fusion processes of Higgs boson production at LEP2.

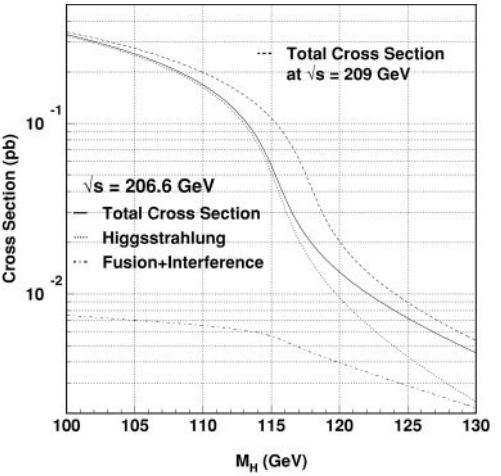

Figure 7 Contributions to the total cross section for Higgs boson production in e^+e^- collisions at $\sqrt{s} = 206.6$ GeV. The total production cross section at $\sqrt{s} = 209$ GeV, the highest center-of-mass energy achieved at LEP, is also plotted.

3.2. Background Processes

Standard-model processes that occurred at LEP are in general well-modeled and thus well-simulated. The main uncertainties in the modeling of background processes are due to higher-order effects, such as the initial-state radiation (ISR) of photons or the radiation of gluons in the final state. Figure 8 shows, for final states containing hadrons, cross-section measurements of standard-model

TABLE 3 Percentage coverage of the channels in the standard-model Higgs search. Expected percentages of Higgs events, based on the total production cross section, are listed for $m_H = 115$ GeV/c^2 and $\sqrt{s} = 206.5$ GeV

Fermions from production process (σ[fb]@$\sqrt{s} = 206.5$ GeV)			**Higgs decay mode (Br[%]@$m_H = 115$ GeV/c^2)**			
Z Decay	**Fusion**	**Interference**	$b\bar{b}$	gg	$c\bar{c}$	$\tau^+\tau^-$
70.1 fb	**3.8 fb**	**2.8 fb**	**74%**	**6.6%**	**3.3%**	**7.2%**
$q\bar{q}$ (69.9% Z Decay)			4-Jet (53.6%)			$q\bar{q}\tau^+\tau^-$ (4.6%)
$\nu_\mu\bar{\nu}_\mu + \nu_\tau\bar{\nu}_\tau$ (13.3% Z Decay)						
$\nu_e\bar{\nu}_e$ (includes WW fusion)			Missing energy (22.8%)			$\tau^+\tau^- + \not{E}$ (2.0%)
6.7%	92.1%	118%				
$\mu^+\mu^-$ (3.4% Z Decay)						
e^+e^- (includes ZZ fusion)			e^+e^-, $\mu^+\mu^-$ (4.9%)			4-Lepton (0.6%)
3.4%	7.9%	−18%				
$\tau^+\tau^-$ (3.4% Z Decay)			$\tau^+\tau^- Hq\bar{q}$ (2.6%)			

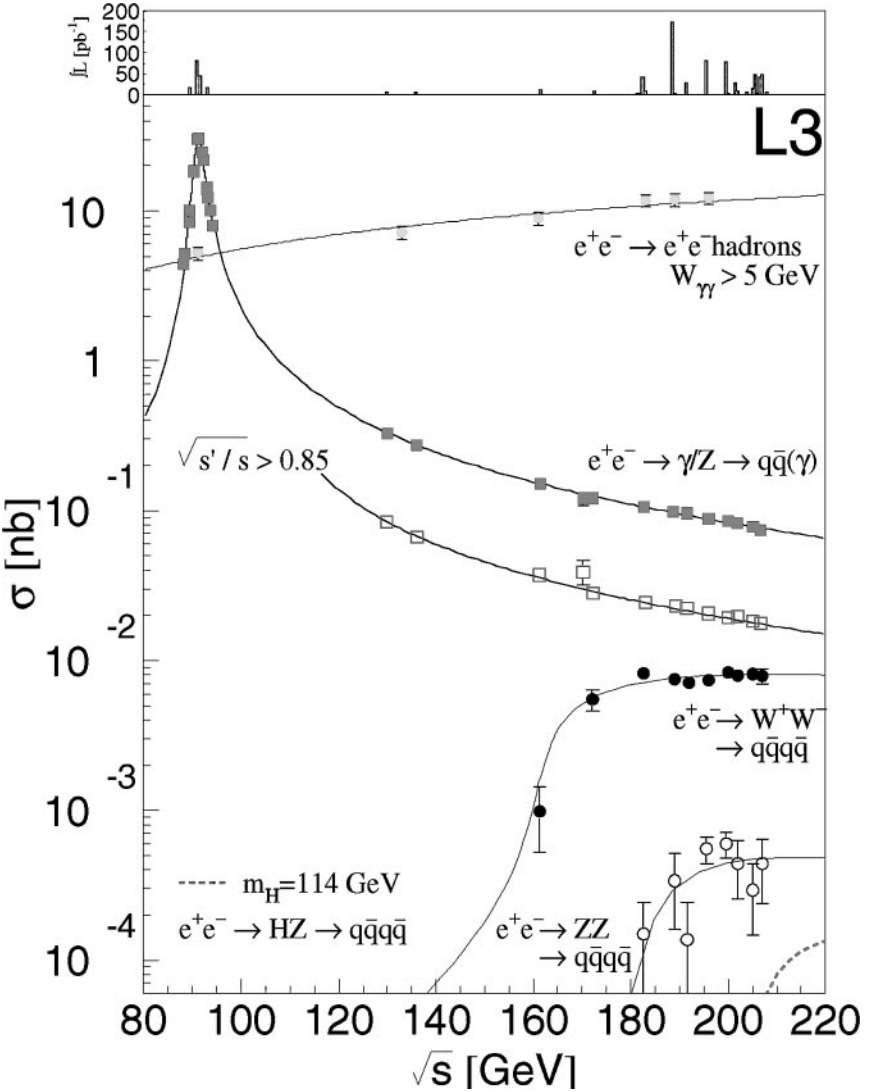

Figure 8 Cross section measurements for final states containing hadrons performed by the L3 experiment over 11 years of LEP operation.

processes by the L3 experiment over 11 years of LEP operation. The hadronic Z peak at $\sqrt{s} \approx M_Z$ is clearly visible. Above the Z peak, only 20% of this $e^+e^- \to q\bar{q}$ cross section produces full-energy $q\bar{q}$ jets in the detector. The remaining 80% contains one or more high-energy photons radiated in the initial state, and the e^+e^- annihilation occurs at the Z mass. Figure 9 shows the background processes for Higgs boson production at LEP.

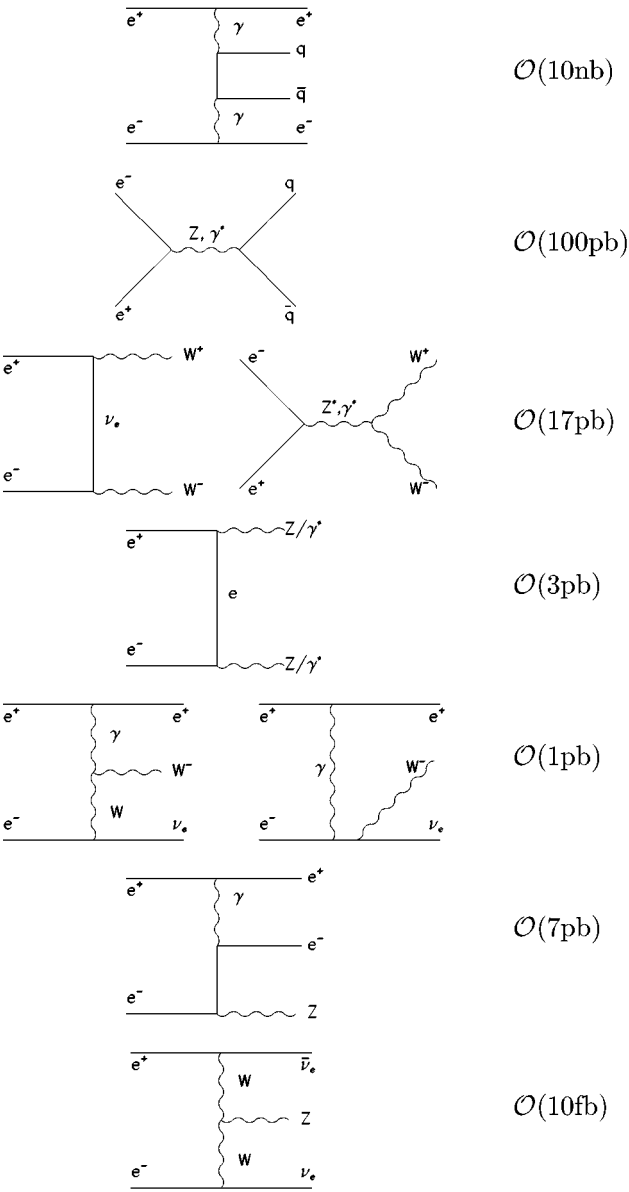

Figure 9 Background processes to the Higgs boson production at LEP2. The typical cross section of these processes for a center-of-mass energy of 200 GeV are given as a guideline; note that some of those figures depend on acceptance and virtuality requirements.

Their relative contribution changes with increasing center-of-mass energy. Above $\sqrt{s} = 161$ GeV, the irreducible four-fermion backgrounds from WW production resemble the energy flow of the Higgs-strahlung process. Fortunately, the near absence of b-quark production in W decays reduces this background substantially. Four-fermion production in the two-photon interactions, although large in cross section, nearly vanishes for large invariant masses and is easily removed from the data. Above $\sqrt{s} = 183$ GeV, ZZ production introduces four-fermion background with b-quark decays. Because both the Z decay properties and the ZZ cross section are very well understood both experimentally and theoretically, the LEP luminosity delivered in 1998 was sufficient to perform the Higgs search in the Z mass range and beyond. In fact, the measurement of the process $e^+e^- \to ZZ \to b\bar{b} + X$ demonstrated the experiments' ability to detect and measure cross sections with b-quark tagging at high energy.

An important aspect of the LEP cross section measurements is the chronological order in which they were made, namely in order of increasing center-of-mass energy. There were many theoretical predictions for enhanced cross sections for WW and ZZ production at threshold, for example, anomalous couplings for WW and extra dimensions in the case of ZZ production. Therefore, when the di-boson production rates were low, the analyses had to rely on the existing measurements and knowledge of the detector response. Accurate verification of these standard-model processes was an ideal training ground for the anticipated $e^+e^- \to HZ$ threshold measurement.

There are a variety of background processes for each channel. Some backgrounds have the same fermions produced in the final state, and others have similar characteristics. Experimental effects such as limited resolution, limited efficiencies, and particle misidentification, or special kinematic configurations can mimic a Higgs signature. The contributions from detector calibration and mismeasurement are kept under control by regularly taking calibration data at the Z peak during each data-taking period. These data samples are primarily used to monitor the b-tag performance, tracking, and calorimeter alignment and calibrations.

3.3. Analysis Procedures

The analysis for each channel concentrates on quantities with distributions that differ for the Higgs signal and background processes. The distinguishing power can vary with Higgs mass and in some cases with the distance to the threshold for Higgs production. Some variables are used to explicitly remove background regions from the event selection. Other variables are used to further separate backgrounds and signal based on the statistical shapes of the distributions, and these are combined to form a final discriminating variable. To quantify the separation power of a channel, the bins of the final variable distribution are treated as independent (until systematic uncertainties are taken into account) Poisson counting experiments. This leads to the construction of a statistical estimator that distributes differently for background-only and signal-plus-background hypotheses.

The statistical estimator used in the LEP combinations is the logarithm of ratio of likelihood functions for the signal-plus-background hypothesis and the background-only hypothesis. Numerically, this consists of a weighted sum over all bins of the distribution, given by

$$-2\ln Q = 2 \cdot s_{\text{tot}} - 2 \cdot \sum_i n_i \ln\left(1 + \frac{s_i}{b_i}\right). \qquad 2.$$

Here i is the index of the bin; n_i, s_i, and b_i are, respectively, the number of observed, expected signal, and expected background events in the bin; and $s_{\text{tot}} = \sum_i s_i$ is the total signal expected. The value of Q constructed in this way is precisely the local likelihood ratio of the signal-plus-background hypothesis to the background-only hypothesis. A negative value of $-2\ln Q$ indicates a preference for the signal-plus-background hypothesis. Because the separation power in the final variable depends logarithmically on the local signal-to-background ratio, the distribution of the final variable rebinned in $\log_{10}(s/b)$ shows directly the most important background regions of the search.

A further discussion of the statistical methods used in the LEP2 Higgs analyses is included in the Appendix.

3.4. Search Channels and Topologies

Of the channels listed in Table 3, only four are used in the standard-model Higgs search: four-jet, missing energy, $\ell^+\ell^-$ pairs ($e + \mu$), and $\tau^+\tau^-$ (see Figure 10). The highest s/b ratio achieved in a search channel depends on the level of analysis optimization and the detector performance. The highest signal-to-background (s/b) ratio achieved in a search channel depends on the level of analysis optimization and the detector performance. A comparison of the average s/b ratio versus the number of expected signal events shows that the four-jet analyses of ALEPH and DELPHI are the most powerful in the high-m_H search (close to 115 GeV/c^2). In particular, these analyses achieve an average s/b ratio greater than unity for a combined expectation of one signal event at $m_H = 115$ GeV/c^2.

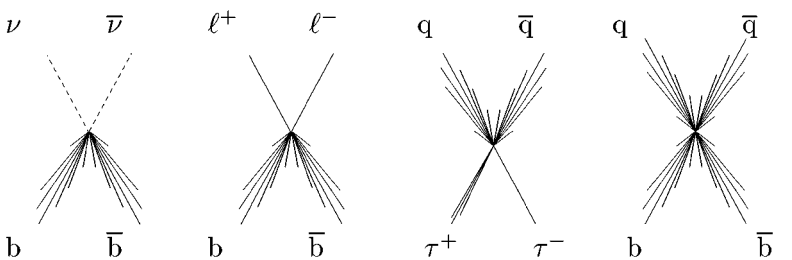

Figure 10 Topologies involved in the search for the standard-model Higgs boson at LEP2, missing energy, lepton pairs, $\tau^+\tau^-$, fan-jets.

3.4.1. FOUR-JET CHANNEL At LEP1, signatures with charged leptons and neutrinos were essential, owing to the overwhelming background in events with hadronic Z decays. At LEP2, at center-of-mass energies well above the Z resonance, this particular background was reduced by more than two orders of magnitude. The four-jet channel, because of its higher branching fraction, thus became the most sensitive topology.

Higgs-strahlung is the only signal process that contributes to the four-jet channel. The resulting topology is two di-jets, one from the decay of the Higgs boson and the other from the decay of a Z boson. In this channel, the Higgs boson is assumed to decay to a pair of b quarks; the resulting jets are therefore expected to be b-tagged. The steric configuration of the jets relies heavily on the Higgs boson mass hypothesis. For low Higgs boson masses (i.e., significantly below the kinematic threshold), each of the di-jets forms a plane, and these two planes do not necessarily coincide. However, when the Higgs boson mass is near the kinematic threshold, the Z and the H are produced almost at rest and the two jets in each di-jet are produced back-to-back, and all jets are in a plane by construction. These geometrical considerations are important for the Higgs boson mass reconstruction.

The three main background processes, $e^+e^- \to ZZ$, $e^+e^- \to W^+W^-$, and $e^+e^- \to q\bar{q}$, have cross sections of orders 1 pb, 8 pb, and 100 pb, respectively. The four-fermion background process does not necessarily lead to a planar topology, whereas the so-called QCD processes, in which a pair of quarks is produced and a pair of gluons is radiated in the final state (or a hard gluon splits to a pair of quarks or gluons), tend to be planar because of QCD dynamics.

When the Z boson decays to a pair of b quarks (referred to as the 4b case), greater signal purity is expected, but so are more jet pairing ambiguities in the case where the Z decays to a light-flavor quark pair (referred to as the 2b case). To profit from the specific features of these two cases, they are treated as independent channels within the four-jet analysis. Independent of the Higgs boson mass hypothesis, for the 4b subchannel the ZZ process is the predominant background; there is also a small contribution from $e^+e^- \to b\bar{b}g$, where the hard gluon splits to a pair of b quarks (Figure 11). In the case of the 2b subchannel, the ZZ process is the predominant background contribution for low Higgs mass hypotheses, but it is only the next-to-highest background near the kinematic threshold. Although it requires either two hard FSR gluons or a FSR gluon splitting (Figure 11), the

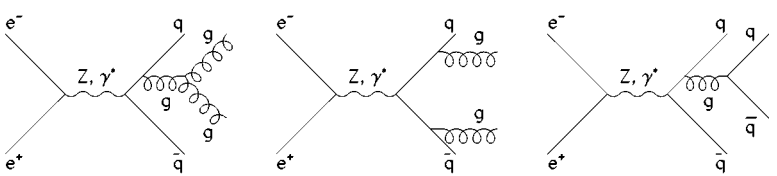

Figure 11 QCD background processes yielding four jets owing to the radiation in the final state of one or more gluons.

$e^+e^- \to b\bar{b}$ is the dominant background to the $2b$ channel for Higgs boson mass hypotheses close to the kinematic threshold; these events tend to yield reconstructed Higgs masses close to the threshold because of their planar topology. The cross section of the W^+W^- process is larger, but it contributes only through b-quark misidentification and even more rarely via CKM suppressed W decays to $b\bar{c}$ or $b\bar{u}$. Four-jet events, especially in the $2b$ channel, offer various handles that help reconstruct the Higgs boson mass. Typically at LEP experiments jet directions were well-measured, whereas their energy measurement suffered from detector effects. In the case of the four-jet channel, assuming the jet directions are well-measured, it is possible to correct for detector effects by rescaling the energies of the jets based on energy-momentum conservation. However, for Higgs boson masses near the kinematic threshold, where events are planar, a kinematic fit is necessary. The further constraint on the recoil to the Z can be either used in the fit or inserted afterward by subtracting m_Z from the sum of the two fitted di-jet invariant masses. These two procedures yield similar results. The typical mass resolution in the four-jet events is $\sim 3\ \mathrm{GeV}/c^2$.

Although the analysis relies mostly on the tagging of b-quark jets and on the mass reconstruction to reach the highest possible sensitivity, event shape variables are also helpful to separate signal and background. All four collaborations use them with multivariate methods such as likelihood ratios or neural networks to exploit the discriminating power of correlations between variables.

3.4.2. MISSING ENERGY CHANNEL The Higgs-strahlung process, in which the Z boson decays to a pair of neutrinos and the Higgs boson to a pair of b quarks, generates two distinct signatures: a large missing mass compatible with the Z mass and two b-tagged jets. This signature also receives contributions from the fusion of W bosons (Figure 6). Although there is constructive interference of the fusion process with Higgs-strahlung, in the final state where the Z boson decays to a pair of electron neutrinos, the contribution from the fusion-plus-interference term is very small. Nevertheless, its role is not negligible, especially for Higgs boson mass hypotheses close to the kinematic threshold.

The missing-energy channel receives background contributions from many processes, but only a few affect this channel seriously. The process $\gamma\gamma \to b\bar{b}$ is not a significant background to the missing-energy channel because of its kinematic characteristics (e.g., its missing mass spectrum is peaked toward very high values). However, the $e^+e^- \to ZZ$ process, in which one Z decays to a pair of neutrinos and the other to a pair of b quarks, is an irreducible and large background to the search for a Higgs boson with mass close to m_Z. The $e^+e^- \to W^+W^-$ process contributes to the background only when one W boson decays semileptonically to a τ and the other decays to a pair of quarks that are mistagged as b jets. The τ decay gives the event a nonzero missing mass, but this background does not heavily affect this channel. The $e^+e^- \to We\nu$ process could be a serious background, since the spectator electron is usually lost along the beam pipe, but the b-jet tagging requirement strongly reduces the small rate because of its relatively small cross section. In the $e^+e^- \to Zee$ process, the spectator electron also

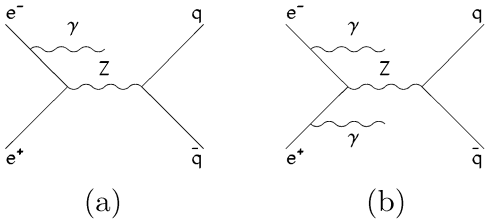

Figure 12 Background processes to the missing-energy final state where one or more photons are radiated in the initial state and escape undetected along the beam line.

escapes detection in the beam pipe; the second electron has low momentum, and the system then resembles a Z production by initial-state radiation (ISR). The process $e^+e^- \to Z\nu\bar{\nu}$ is also irreducible when the Z boson decays into b-quark jets, for Higgs boson masses near m_Z, but this process has an almost vanishing cross section. As in the four-jet channel, the most tedious background near the kinematic threshold is not of the four-fermion type, but rather $e^+e^- \to q\bar{q}$ where the missing mass is due to two ISR photons emitted at low angle and lost along the beamline (as shown in Figure 12*b*), one ISR photon (as illustrated in Figure 12*a*) and a mismeasurement in the jet energy, or simply two mismeasured jet energies. Furthermore, this background tends to peak near the threshold in reconstructed mass, which is an artifact of the mass reconstruction algorithm. In the missing-energy channel, the two jet energies cannot be rescaled independently because of the lack of kinematic constraints. In this case, only the recoil to the Z mass can be used. The visible mass is rescaled with a single parameter, which is equivalent to applying a unique rescaling coefficient to the four-momentum of both jets. The typical peak resolution is of the order of 3 GeV/c^2, comparable to the four-jet channel. But in this channel and especially for Higgs boson masses near threshold, where the fusion-plus-interference contribution can add up to almost half of the total signal cross section, this resolution is degraded by large and wide tails.

3.4.3. $\ell^+\ell^-$ CHANNEL The topology of the lepton channel is a pair of electrons or muons and a pair of b-quark jets. This is a very distinctive signature, but it has a very small rate because of the small branching of the Z to electrons and muons, and, to a much lesser extent, because of the interference between the Higgs-strahlung production and ZZ fusion, which is destructive.

The backgrounds to this channel originate almost exclusively from the $e^+e^- \to ZZ$ process. Practically none of the other processes can yield a similar topology. Its rejection relies greatly on the mass reconstruction and on the tagging of b-quark jets. The Higgs boson mass is reconstructed from the recoil to the two-lepton system.

3.4.4. $\tau^+\tau^-$ CHANNEL The topology in the $\tau^+\tau^-$ channel is a pair of tau leptons and a pair of jets. This channel is separated from the $\ell^+\ell^-$ channel for two main

reasons. First, the invariant mass of the $\tau^+\tau^-$ pair cannot be accurately measured because of the unmeasured energy carried by the neutrinos of the $\tau^\pm$ decays; the mass reconstruction procedure is thus very different from that used in the lepton channel but is actually very similar to that used in the four-jet channel. The second reason is that this channel also receives contributions from the $Z \to b\bar{b}$ and $H \to Z^+Z^-$ events.

3.5. Lower Limit on the Higgs Mass Before 2000

The data collected through the end of 1999 were recorded up to a maximum center-of-mass energy of $\sqrt{s} = 201.6$ GeV and yielded no indication of the production of a Higgs boson. Figure 13 shows the consistency of the data with the expected distribution for the background hypothesis. The data are in good agreement with the background-only expectation, which indicates an accurate understanding of the background rates. The exclusion of the Higgs boson in the confidence level for signal (CL_s) is also shown in Figure 13, where the lower limit on the Higgs boson mass is set at $m_H = 108.6$ GeV/c^2 at the 95% confidence level for a median expected limit of $m_H = 109.1$ GeV/c^2 (31–34). The drop-off of CL_s is dramatic below 107 GeV/c^2, showing that the observed 95% exclusion limit at 108.6 GeV/c^2 for a median expected limit of 109.1 GeV/c^2 is a reference point for a very rapid, unambiguous exclusion for lower masses. The search data continue to yield no preference for a signal up to and beyond the production threshold $m_H \approx \sqrt{s} - 91.2 \approx 110.4$ GeV/c^2.

The LEP Higgs search program, having substantially surpassed the *ZZ* production threshold in 1999, looked to the LEP machine group for the continued increase in beam energy and luminosity performance in 2000.

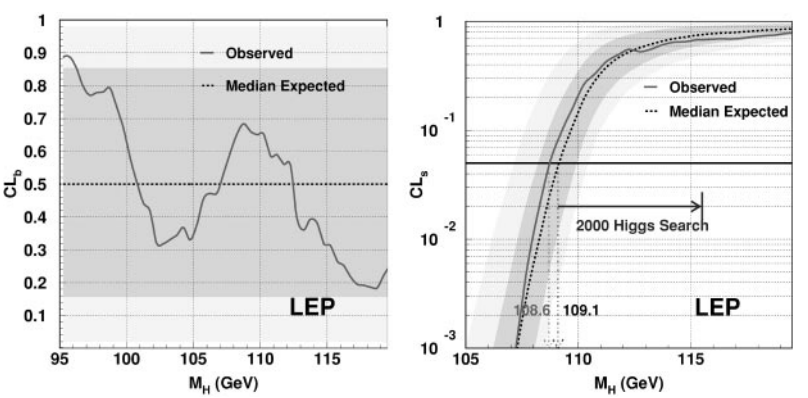

Figure 13 LEP data up to 2000: as a function of the Higgs boson mass, m_H, the confidence level for (*a*) the background and (*b*) the signal.

4. PUSHING LEP TOWARD AND BEYOND ITS LIMITS

Because 2000 was announced to be the final year of LEP operation, a special effort was made to push the machine toward its limits to obtain a significant amount of luminosity at the highest possible energy, thereby extending the sensitivity to a higher Higgs boson mass.

Most of the ideas to increase the energy or luminosity of the machine presented in this section were presented at the Chamonix Workshop (35). Amazingly, all these improvements proved to be effective and LEP not only reached but surpassed the initial goals.

4.1. Strive to Reach the Highest Energies

The center-of-mass energy of a circular e^+e^- collider is limited by the magnetic field of the dipole magnets and the RF power available to compensate for the synchrotron radiation losses. The synchrotron radiation energy loss, which is proportional to the fourth power of the beam energy, is the limiting factor. Within its effective radius of $\sim$3 km and with the dipole field strength ranging between 0.01 and 0.2 Tesla, the maximum center-of-mass energy relies mainly on the accelerating gradient. Four of the eight straight sections were instrumented with accelerating devices. The total number of accelerating RF cavities available was 288 (36).

The design accelerating gradient of each superconducting RF cavity was 6 MV/m. Running at this nominal gradient with the entire batch of RF cavities allowed LEP to reach a center-of-mass energy of 192 GeV. At this energy, the sensitivity of Higgs boson searches at LEP was about 100 GeV/c^2. A series of upgrades and ingenious ideas allowed LEP to surpass the design capabilities.

- The cryogenic facilities were upgraded, allowing the cavities to be conditioned at up to 7.5 MV/m. The overall gain in gradient obtained from this change was 650 MV. The upgrade also improved the stability of the cryogenic system. This improvement allowed the center-of-mass energy to reach 204 GeV and enabled LEP to be sensitive to a Higgs boson with a mass of 112 GeV/c^2.
- The average time between klystron trips at LEP was about one hour. To maintain stable beams, it was therefore necessary to operate with a margin of at least two klystrons (200 MV), i.e., allowing two klystrons to trip simultaneously without losing the beam. However, with the improved stability, it appeared to be possible to run with a margin of only one klystron (100 MV) without greatly increasing the beam losses. The margin mode of one klystron gained 1.5 GeV in center-of-mass energy and about 1 GeV/c^2 in sensitivity to the Higgs boson.
- Reducing the nominal 350 MHz RF by $\sim$100 Hz resulted in a small shift of the beam orbit. As a result, the beams were exposed to the dipole component

of the focusing quadrupole magnets. The smaller frequency also allowed shorter bunches and therefore increased the available RF margin. The use of a lower frequency allowed a gain of 1.4 GeV in center-of-mass energy and 600 MeV/c^2 in sensitivity to a Higgs boson.

- Unused orbit correctors were powered in series to act as dipoles, so as to increase the effective bending length. This change allowed an increase in center-of-mass energy of 400 MeV and improved the Higgs boson mass sensitivity by 250 MeV/c^2.
- Eight copper cavities from LEP1 were reinstalled for an additional gain in RF gradient of 30 MV, which resulted in an increase of 400 MeV in center-of-mass energy and 250 MeV/c^2 in sensitivity to a Higgs boson.

All these improvements led to an increase in energy of ∼15.7 GeV. LEP was able to run in quite stable conditions at a center-of-mass energy of ∼207 GeV.

4.2. Strive to Reach the Highest Luminosities

When the total current reaches a certain threshold, the RF system becomes unstable, resulting in an exponential increase of the number of trips per hour.

At LEP2, the strong radiation damping left the beams very stable, and the coast duration was no longer limited by beam-beam interactions as was the case at LEP1. Instead, the stability of the beams was mainly governed by the available RF margin. Reaching the highest possible luminosity was therefore a trade-off between the higher center-of-mass energy and the stability of the beams and the fill time.

During the last day of operation in 1999, it was proven that the beam energy could be increased within a fill, in a short period of time (typically a few minutes), without increasing the background in the detectors. This “mini-ramp” technique allowed the machine to run at the highest energy, with no RF margin. As shown in the following subsection, this technique had an important impact on the sensitivity to a heavy Higgs boson.

The smaller the margin, the smaller the coast lifetime, and the more important it was to minimize the turnaround time. After each beam loss, a great effort was made to accelerate all the inter-fill steps, such as the setup (e.g., degaussing less), the injection, the energy ramp, and the beam adjustment.

4.3. Optimizing LEP for the Highest Sensitivity to the Higgs Boson

It was concluded at the Xth Chamonix Workshop (35) that the best scheme was to operate LEP with one klystron margin for about one hour and then mini-ramp to no margin until the first klystron tripped.

This scheme was optimal not only for the Higgs search but also for the search for charginos, which is essentially driven by the largest possible center-of-mass

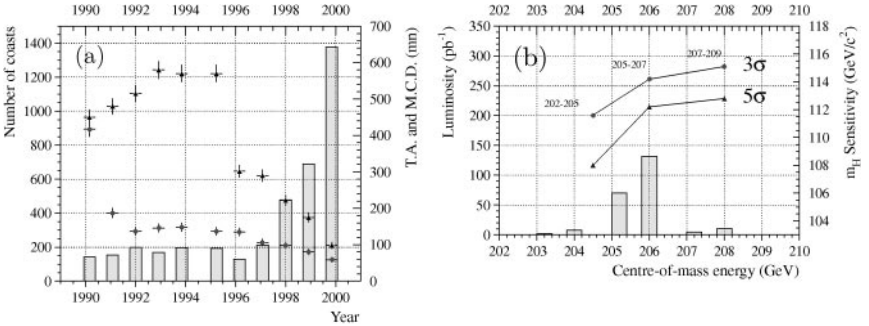

Figure 14 (*a*) Total number of coasts, mean coast duration (MCD; in minutes), and average turnaround time (TA; in minutes) for each running year. (*b*) Total integrated luminosity collected at each center-of-mass energy in 2000. The corresponding increase in 3σ (points) and 5σ (triangles) sensitivity to the standard-model Higgs boson is also indicated.

energy and for which only a small amount of data (of the order of 10 pb^{-1} per experiment) was required.

4.4. Synopsis of the Running of LEP in 2000

The performance of LEP had been constantly improving over the years. The total delivered luminosity and the peak luminosities have increased almost every year. The total luminosity in 2000 was slightly smaller than in 1999 as a result of the optimization. Figure 14*a* emphasizes the changes in the LEP operations in 2000, showing the number of coasts, the average coast duration, and the average turnaround time. In 2000, there were 1377 fills of an average coast duration of 98 min; the record fill time was 59 min.

Figure 14*b* shows the distribution of luminosities delivered at each center-of-mass energy in 2000. The corresponding effect on the 3σ and 5σ sensitivities of the Higgs boson search are also indicated therein. It should be noted that the small amount of data accumulated at the highest center-of-mass energy allowed the 3σ sensitivity to increase by $\sim$1 GeV/c^2. This effort ultimately allowed the searches for the Higgs boson to reach a sensitivity of 115 GeV/c^2.

5. HINTS FOR THE PRODUCTION OF THE STANDARD-MODEL HIGGS BOSON AT LEP

5.1. Chronology

In the year 2000, the LEP machine extended the reach of the Higgs boson search by roughly 6 GeV. By midsummer, 30 pb^{-1} of data had been collected per experiment

at $\sqrt{s} \approx 206.6$ GeV. One high-mass candidate [called candidate (c)] was observed in the four-jet channel with reconstructed mass 114 GeV/c^2. However, since no other candidates were observed in this range, the rate was consistent with the background-only hypothesis.[3]

By September 5, 2000, two more candidates were recorded by ALEPH in the four-jet channel. The ALEPH data, combined with those of DELPHI, L3, and OPAL, favored the signal-plus-background hypothesis with a best estimate for the Higgs mass of $m_H = 114.9$ GeV (38). The exclusion limit from the DELPHI-L3-OPAL combination could rule out Higgs masses below 114.2 GeV/c^2, not a 114.9 GeV/c^2 signal. Similarly, a combination of all the search channels excluding the four-jet channel was limited in sensitivity to $m_H < 113.3$ GeV/c^2. A comparison of the search-channel expected performances across experiments showed that the ALEPH four-jet channel had the greatest sensitivity to high-mass signals. Based on the excess observed with 70 pb^{-1} of data at $\sqrt{s} \approx 206.6$ GeV, estimates were computed on the expected significance with two additional months of LEP running.[4] A doubling of the data was sufficient to test whether other experiments and other channels observed high-mass candidates. Complementary to the selection of high-mass candidates was the expected observation of an overall excess of 12 events or more in the intermediate s/b region of the search. By November 3, 2000, the closure date of the LEP2 program, the LEP machine delivered 70% more data at $\sqrt{s} \approx 206.6$ GeV to the four experiments. With the additional data, L3 and OPAL showed moderate increases in CL_{s+b} at high mass, with a significant high-mass Higgs candidate recorded by the L3 experiment in the missing energy channel. Figure 15 shows the $\log(s/b)$ distribution of the LEP data at $m_H = 115.6$ GeV/c^2. Table 4 shows the number of events selected after several s/b cuts for $m_H = 115.6$ GeV/c^2 compared with expectations for background-only and signal-plus-background, showing a data excess in the high- and low-s/b regions of the search.

The LEP data establish a 95% exclusion limit up to $m_H = 114.0$ GeV/c^2 and a hint of an excess at $m_H = 115.6$ GeV/c^2. Figure 16*a–b* compares the LEP exclusion limit in CL_s with the 1999 result.[5] Figure 17 compares the $-2 \ln Q$ distribution of the data to the expected observation from a $m_H = 115.6$ GeV/c^2 signal. An excess of two standard deviations from background is found for this mass hypothesis. The data show an excess over a broad range of mass hypotheses, as is predicted by the curve for the fixed mass signal. The expected distributions of observations for $m_H = 115.6$ GeV/c^2 for background-only and signal-plus-background are also indicated in Figure 17. There is a 3.4% probability that the observed data are

[3]The recommendation given to the scientific board (LEPC) of the LEP program at the July meeting was to reoptimize the LEP running for the chargino search because the Higgs search was negative.

[4]In the presence of a $m_H = 115$ GeV/c^2 signal, the observed $1 - CL_b$ significance was predicted to be in the 68% interval [0.003%, 5.3%] for a doubling of the luminosity.

[5]The LEP data are still preliminary awaiting final publications from the experiments.

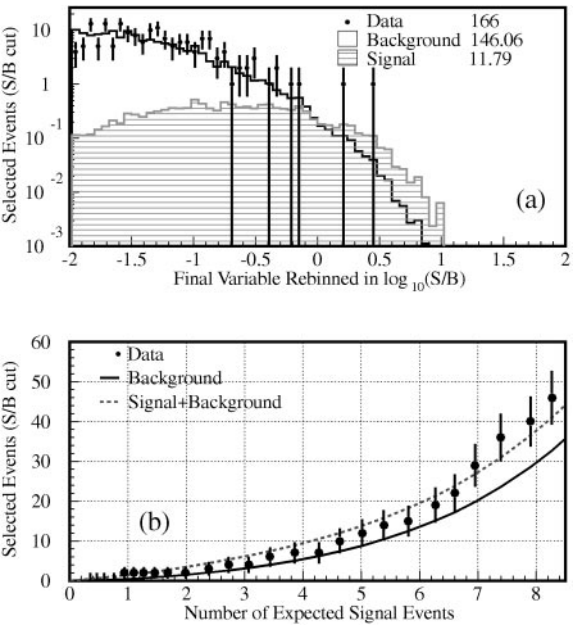

Figure 15 (*a*) The $\log(s/b)$ distribution of the combined LEP data at $m_H = 115.6$ GeV/c^2. (*b*) The cumulative distribution integrating from high-s/b to lower values.

compatible with the background-only hypothesis and a 44% confidence level for signal-plus-background (39).

The search data can be decomposed into contributions by experiment and by channel. Figure 18*a* shows that, for the background-only hypothesis, ALEPH is the only individual experiment with a significant excess. Similarly, comparing the data by channel, the four-jet channel, as shown in Figure 18*b*, contains the most

TABLE 4 The number of events and the likelihood estimator values in data compared with expected numbers for the background-only and signal-plus-background hypotheses for $m_H = 115.6$ GeV/c^2[a]

Search sample selection	Number of events			$-2\ln Q$ values [68% interval]		
	Data	Bkgd.	Sig. + Bkgd.	Data	Bkgd.	Sig. + Bkgd.
All Events	1117	1143.8	1158.7	−3.2	3.3 [6.6, 0.1]	−4.2 [0.4, −8.8]
$s/b > 0.05$	80	60.1	70.3	−3.3	3.2 [6.4, 0.0]	−4.1 [0.4, −8.7]
$s/b > 0.3$	10	7.5	12.1	−0.5	2.6 [5.3, −0.2]	−3.4 [0.8, −7.6]
$s/b > 1.0$	2	0.8	2.3	−1.1	1.3 [2.9, −0.6]	−1.9 [1.3, −5.2]

[a]The search sample ranges from the full selected sample to a restricted set of high-signal-over-background analysis regions. The $s/b > 1.0$ sample has slightly less search sensitivity than the complementary $s/b < 1.0$ set of search data.

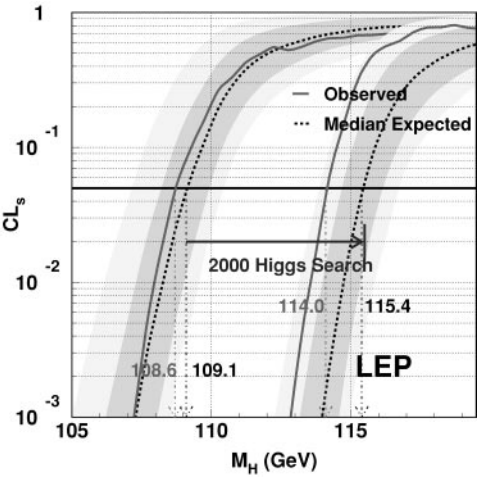

Figure 16 The expected and observed confidence levels for signal, CL_s, for the 2000 data compared to the 1999 data. The observed CL_s at $m_H = 115.4$ GeV/c^2 is eight times higher than the median expectation from background events.

significant excess. On the other hand, with regard to a signal-plus-background hypothesis, the data from the experiments show a balancing of the ALEPH excess with that of DELPHI. Figure 18*c* compares the data by experiment in the vicinity of a $m_H = 115.6$ GeV/c^2 Higgs boson signal (40–45). Correspondingly, the comparison of the data by channel in Figure 18*d* shows that a prominent four-jet excess

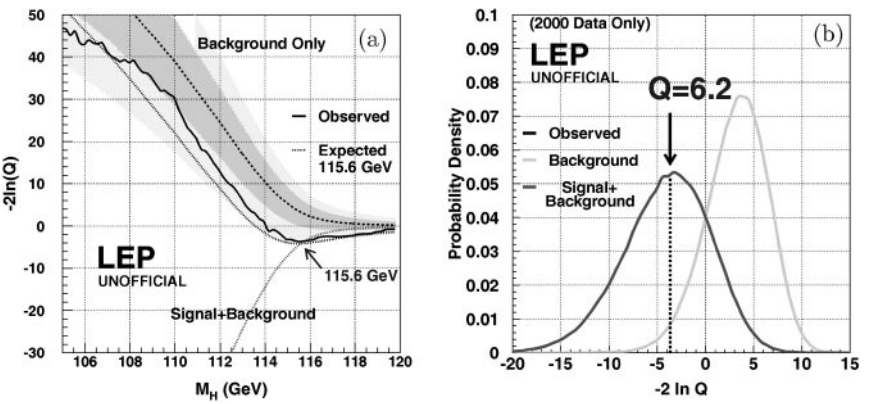

Figure 17 (*a*) Observed values of $-2 \ln Q$ as a function of Higgs boson mass are compared with the background-only expectation and the prediction for background with the addition of a 115.6 GeV/c^2 signal. (*b*) Distributions of expected observations for the two hypotheses at $m_H = 115.6$ GeV/c^2 are compared to the LEP observation.

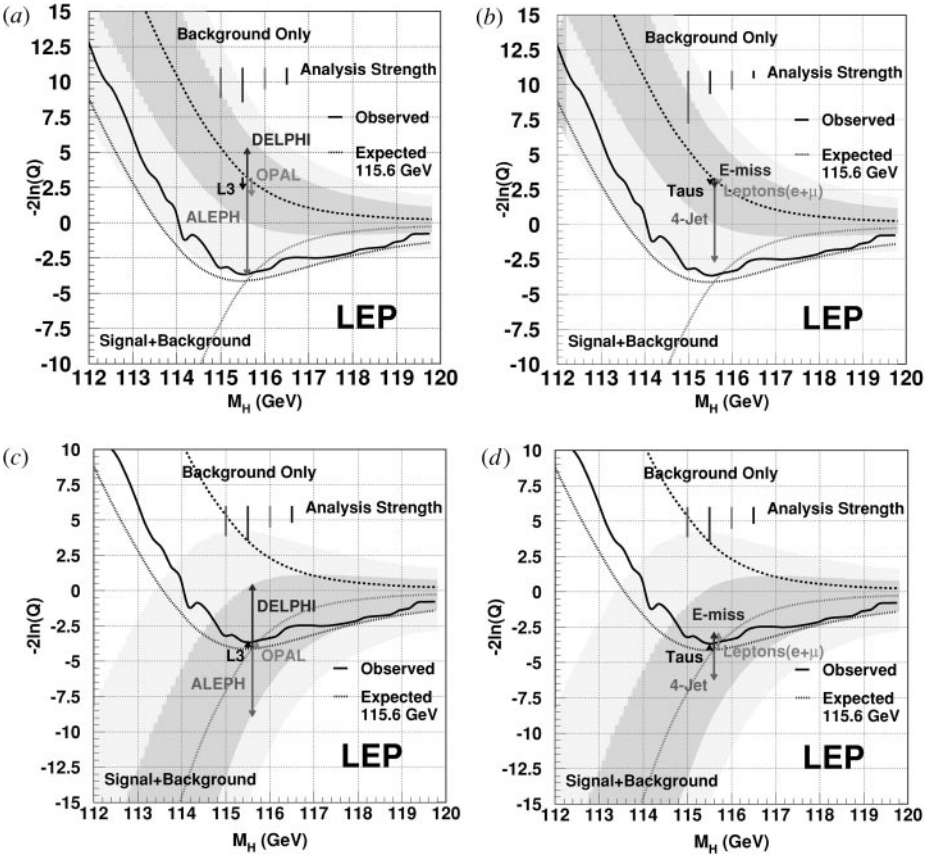

Figure 18 The search data decomposed into contributions by experiment (*a*) and by channel (*b*) are compared to the background-only hypothesis. Plots *c* and *d* compare the same decomposition to the signal-plus-background hypothesis.

relative to the other search channels is expected in the presence of a signal, given the relative strengths of the analyses.

The mass resolution of the excess at $m_H = 115.6\,\mathrm{GeV}/c^2$ is estimated from the expected signal distributions. In general, the mass range of $-2\ln Q$ values that are within 1 unit of the observed minimum gives the approximate 68% interval for the best estimate of the Higgs mass. The estimate based on the expected signal distribution, scaled to the observed minimum, yields a value of $m_H = 115.6^{1.5}_{-1.1}\,\mathrm{GeV}/c^2$, as shown in Figure 19. Rescaling the channel-by-channel distributions in luminosity to obtain the same overall sensitivity of the combined search shows that the four-jet channel has the highest mass resolution of $[-1.1, 1.2]\,\mathrm{GeV}/c^2$ whereas the missing energy has the lowest resolution of $[-1.3, 2.3]\,\mathrm{GeV}/c^2$. The relative contribution of the channels to the search follows the overall efficiencies as indicated in Table 3 with the exception of the lepton ($e + \mu$) channel, which

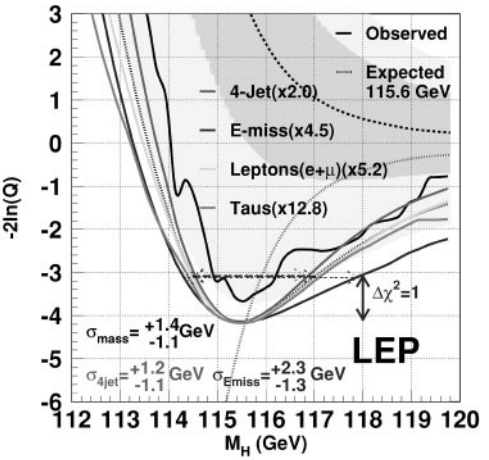

Figure 19 Estimation of the mass resolution of the excess at $m_H = 115.6$ GeV/c^2. The expected signal distribution has been rescaled to match the observed minimum.

is more sensitive by a factor of four owing to low backgrounds and high mass resolution.

5.2. Mass Plots

The result of the searches can also be illustrated in terms of reconstructed mass plots. To equitably depict the results of all experiments and all channels, a common purity level is requested. The criterion for purity is the expected signal-to-noise ratio at large reconstructed masses. Figure 20 displays the combined mass plots of the searches, with various requirements on the purity.

The number of background and signal events expected and the number of data candidate events observed at all the purity levels and mass domains illustrated in Figure 20 are summarized in Table 5. The numbers of observed events are clearly more consistent with the numbers of events expected in the signal-plus-background hypothesis than in the background-only hypothesis. The agreement with the signal-plus-background expectation is observed over the full spectrum, at large masses, and at all purities. It is this consistency at different purity levels that translates into an improbable compatibility of the observation with standard-model backgrounds.

5.3. Significant Events

Table 6 lists the 11 most significant events collected at LEP in 2000. As expected, the largest fraction of events expected with high weights consisted of four-jet events. Of the 11 events with an s/b value greater than 0.4, eight were four-jet candidates. Four were observed by ALEPH, two by OPAL, and two by DELPHI. One event was a missing-energy candidate observed by the L3 experiment. The two remaining events were from the lepton and the $\tau^+\tau^-$ channels. The

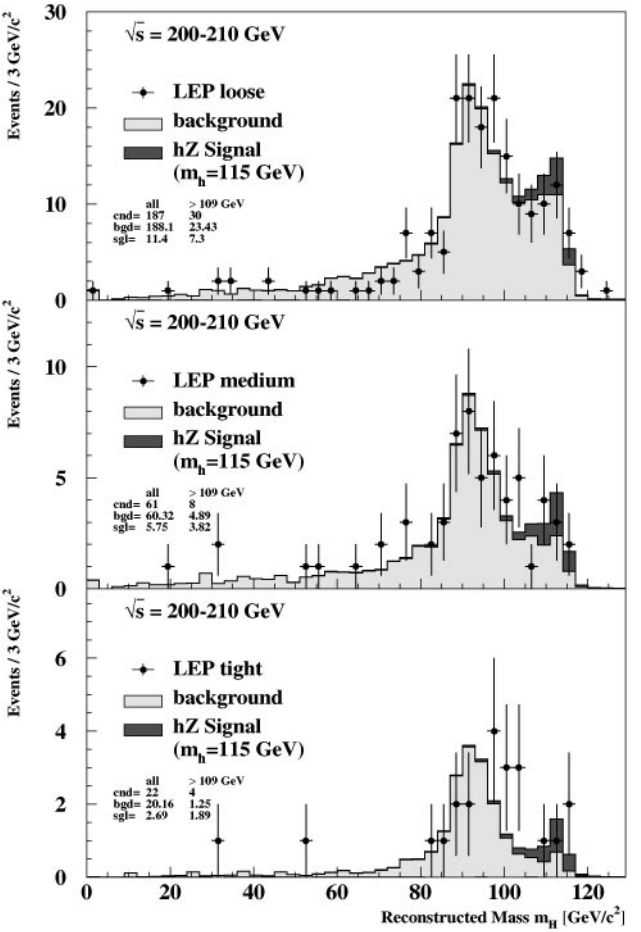

Figure 20 Combination of the reconstructed mass distributions for all channels and all experiments for various levels of signal over expected background.

two foremost candidate events deserve closer examination. The high-significance missing-energy candidate has been a subject of debate.

The most significant candidate (40), known as (c), is shown in Figure 21. Besides its large weight (based on *b* tag, shape variables, and reconstructed mass), other quantitative and qualitative aspects support its leading position in terms of significance. For example, the jets corresponding to the pairing attributed to the Higgs boson have unambiguous displaced vertices. The 13.8 GeV/*c* missing momentum points to the direction of the jet with a clearly identified muon, which indicates a heavy-quark semileptonic decay. Furthermore, the muon originates from the secondary vertex. The measured invariant mass of the pair of jets with

TABLE 5 The number of background and 115 GeV/c^2 signal events expected and the number of candidate events at different levels of purity, for the full spectrum of reconstructed mass and for a domain enriched with signal ($M_{rec} > 109$ GeV/c^2)

	Full spectrum			$M_{rec} > 109$ GeV/c^2		
Purity	**0.3**	**1**	**2**	**0.3**	**1**	**2**
Bkgd.	188.1	60.3	20.2	23.4	4.9	1.2
Sig.	11.4	5.7	2.7	7.3	3.8	1.9
Data	187	61	22	30	8	4

displaced vertices, taking into account the missing momentum within the jet containing a muon, is 114.4 GeV/c^2. The energies of the two remaining jets are 43.5 and 49.0 GeV, respectively, typical of the decay of a Z nearly at rest.

The second most significant candidate (40), candidate (b), is selected as a four-jet event. This candidate has also been a subject of discussion because of a 22 GeV electromagnetic shower observed in the very forward direction. An electromagnetic deposition at low angle is usually attributed to the radiation of a photon in the initial state, which would tarnish this golden candidate if it were not for the compelling evidence that this energy deposit is not related to the event. The total large measured visible energy is 252 GeV. Such a large value can hardly be explained by

TABLE 6 Highest-purity candidate events, their reconstructed mass, the center-of-mass energy at which they have been collected, and their weight

Experiment	**Channel**	$\sqrt{s}$	M_{rec} (GeV/c^2)	$(s/b)_{115}$
ALEPH[c]	4-Jet (2b)	206.7	114.3	4.6
ALEPH[b]	4-Jet (4b)	206.7	112.9	2.3
ALEPH[a]	4-Jet (4b)	206.7	110.0	0.9
L3[α]	$E_{missing}$	206.4	115.0	0.7
OPAL	4 Jet (2b)	206.7	110.7	0.7
DELPHI	4 Jet (4b)	206.7	114.3	0.6
ALEPH[*]	Electrons	205.0	118.1	0.6
ALEPH	Taus	208.1	115.4	0.5
ALEPH[d]	4 Jet (2b)	206.5	114.5	0.5
OPAL[*]	4 Jet (4b)	205.4	112.6	0.5
DELPHI	4 Jet (2b)	206.7	97.2	0.4

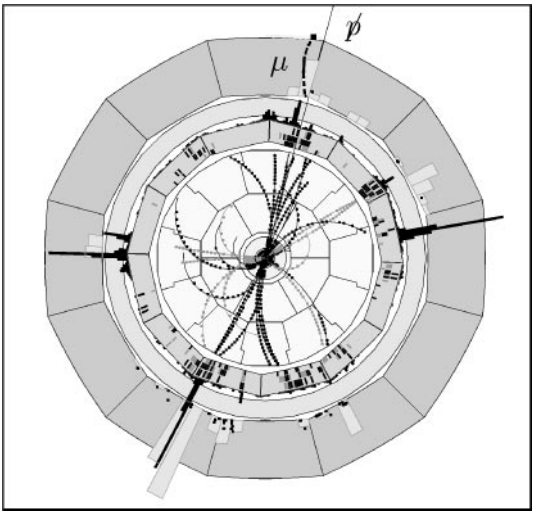

Figure 21 Event display of ALEPH candidate (a) in the $(r\phi)$ transverse view.

a fluctuation in the visible energy resolution, which is of the order of 10 GeV. An energy of 22 GeV is typical for beam-related background as measured in events collected at random beam crossings, and the momentum imbalance of the event is in the opposite direction. These observations strongly support the assignment of this low-angle electromagnetic object to beam background. Removing it increases the reconstructed mass from 112.9 GeV/c^2 to 114.5 GeV/c^2. Furthermore, a fit of the most probable ZZ pairing choice yields large Z boson masses of 94.0 GeV/c^2 and 97.3 GeV/c^2. The best background explanation for this event, $e^+e^- \to ZZ$, is therefore unlikely.

The weight of the candidate event (a) is discussed in Reference (40) and is also shown to be well-justified.

At first sight, the L3 candidate (43) known as (α) seems to be the perfect missing-energy event near threshold (Figure 22). It has two jets back-to-back and a low value of transverse momentum, and it is well b-tagged. Actually, for a Higgs boson produced near threshold, the Z boson is produced somewhat off-mass-shell (by $\sim$1 GeV/c^2). The resulting topology is two slightly acollinear jets. Such topology is precisely what would be expected from the $e^+e^- \to Z^* \to q\bar{q}$ process, in which the two jets fluctuate low. The two jets of candidate (α) are very collinear. However, the hypothesis of a nonradiative $q\bar{q}$ background is strongly disfavored by the fact that the event transverse momentum is small, which would require that the fluctuation of the two jets be balanced. The double-radiative hypothesis is also disfavored by the fact that the event is very collinear, which requires that the photons lost along the beam line be balanced.

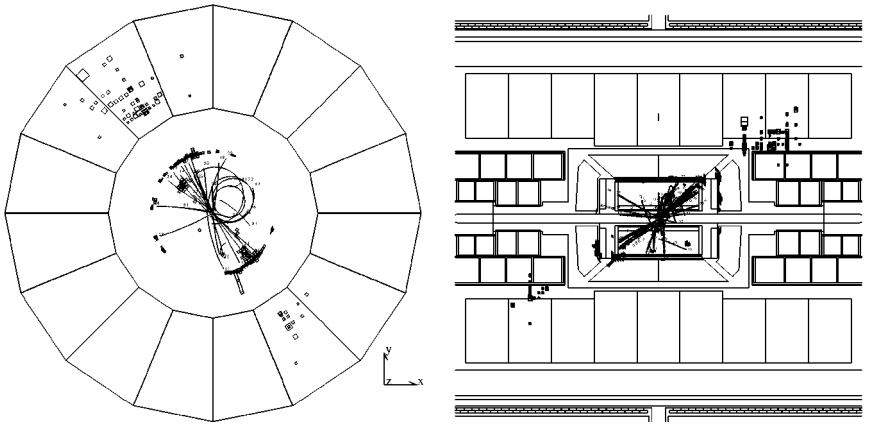

Figure 22 L3 candidate (α) in the transverse ($r\phi$) (left) and longitudinal (rz) (right) views.

Candidate (α) is atypical. The event is very compatible with the signal hypothesis, but it is not from the highest region of the signal phase space. It is most clearly distinguished by its improbability to come from known standard-model backgrounds.

5.4. Systematic Studies and Robustness of the Search

5.4.1. SYSTEMATIC UNCERTAINTIES The study of systematic uncertainties in the search for Higgs bosons at LEP became particularly important when the analyses required background subtraction to overcome the irreducible $e^+e^- \to ZZ$ background at center-of-mass energies of 183 and 189 GeV. The treatment of systematic uncertainties in the context of subtraction is an extension of the method described in References (53) and (54), where all sources of systematic uncertainties are treated with a Gaussian smearing of the nominal background and signal values in the computation of the likelihood probability density. This treatment assumes that all systematic sources originate from resolution-like effects. As a consequence, its impact on the final result is very small. It is far more crucial to identify systematic biases that must be corrected for, especially if an excess is observed.

The largest contribution to the systematic uncertainties is due to the modeling of backgrounds and particularly the limited statistics of the simulation, which in some cases can reach the relative level of 10%. The other typical sources of systematic uncertainties and their effect on the background levels are (*a*) detector response resolution (calorimeter energy, tracking, and impact-parameter resolutions can also be treated as corrections, and when treated as uncertainties, their effect amounts to 2–5%); (*b*) the hadronization of *b*-quark jets, for instance, through the modeling of their fragmentation, their particle multiplicities, and the mass of the *b* quark (these uncertainties apply to backgrounds at the level of 2–3%); and (*c*) the cross-section measurements, which have an impact as low as 1%. The uncertainties on signal

efficiencies are essentially related to the tagging of *b*-quark jets and typically range between 1% and 3%.

To thoroughly assess the systematic corrections related to the detector response that can vary with time, each year a control sample of data at the Z peak has been collected. Both the jet energy and the *b* tagging are calibrated with these data samples. The jet-energy and angular-resolution corrections are very small. The tagging of *b*-quark jets, being sensitive to very small variations in alignment, requires a careful calibration. One successful calibration method is the single-tag/double-tag method used to measure R_b, the Z pole observable defined as $\tau(b\bar{b})/\tau$ (hadrons), where the tagging efficiencies are measured in Z decays using the standard-model prediction of R_b. Another way to calibrate the analysis performance is to correct for the impact-parameter resolution effects by smearing the track parameters.

The robustness of the observation of the excess in 2000 resides mostly in the absence of unexpectedly large biases in the numerous systematic studies carried out after the original analyses and in the fact that such large biases had never been observed in previous LEP Higgs boson searches. However, various control samples at high center-of-mass energies were selected to further support the robustness of the searches.

5.4.2. HIGH-ENERGY CONTROL SAMPLES The numerous control samples at high center-of-mass energy illustrate the fact that Higgs searches at LEP concentrated on well-described background distributions, which were not subject to uncontrolled tails. Below, examples demonstrate the robustness of the two most delicate issues in the searches for the Higgs boson.

The first is the tagging of *b*-quark jets. The modeling of the *b*-tagging algorithms calibrated at the Z peak is evaluated both on Z events produced by ISR and semileptonic WW decays, the latter being deprived of signal. Figure 23 illustrates the quality of the simulation in both control samples in ALEPH data (40).

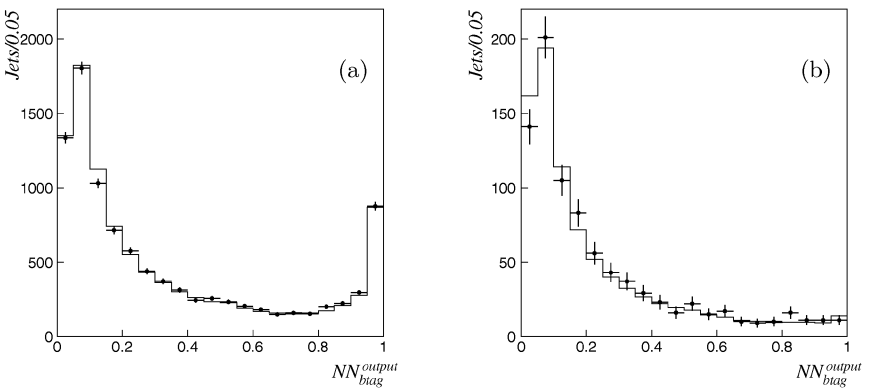

Figure 23 ALEPH *b*-tagging NN output (*a*) in radiative-return Z events and (*b*) semileptonic WW events, for data (points) and Monte Carlo simulation (histogram).

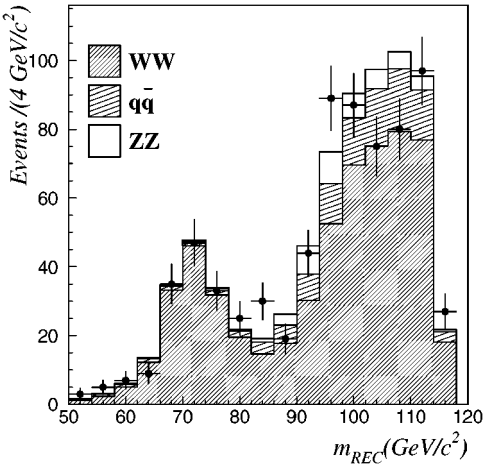

Figure 24 ALEPH reconstructed mass distribution for a control sample of events, where a *b*-tag veto is applied to select mainly $e^+e^- \rightarrow W^+W^-$ events, for data (points) and Monte Carlo simulation (histogram).

The second is the modeling of the mass reconstruction procedure in the four-jet channel, where most of the excess is observed. This is evaluated with a sample of background events that have a topology similar to that of the signal. These events are mainly $e^+e^- \rightarrow W^+W^-$ events selected by applying typical four-jet topological cuts and a *b*-tag veto. Figure 24 shows the reconstructed mass distribution of such events selected by the ALEPH experiment. The low mass peak at masses around $\sim 2m_{W^\pm} - m_Z$ corresponds to the correct choice of jet pairing. The peak of events at higher reconstructed masses corresponds to events with the wrong pairing. Good agreement between data and Monte Carlo simulation over the entire spectrum is observed, which further supports the quality of the reconstructed mass modeling and disfavors the possibility of a systematic bias.

5.5. The ALEPH Four-Jet Events

So far, the reported results of the ALEPH experiment were obtained with an analysis based mostly on neural-network techniques and two discriminating variables. To further substantiate this result, ALEPH also performed an analysis based on sequential cuts in which the event weight is determined only with the use of the reconstructed mass as a discriminating variable (40). Both analysis streams yield very similar combined results, but the weight of each individual candidate event is different (see Figure 25) because a single discriminating variable is used. In the approach with sequential cuts, all the ALEPH candidate events listed in Table 6, namely (a), (b), (c), and (d), are selected. One additional candidate event, (e), is selected. The consistency of the overall results in the ALEPH four-jet channel confirms the robustness of the search.

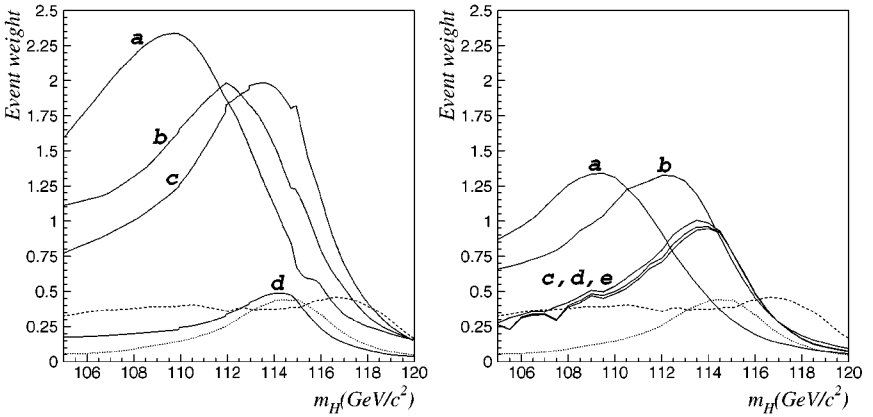

Figure 25 Distributions of the weights as a function of the Higgs mass hypothesis of the most significant candidate events collected by the ALEPH experiment in the neural-network (*a*) and cut analysis streams (*b*).

6. SEARCHES FOR HIGGS BOSONS BEYOND THE STANDARD MODEL

Finding hints of the presence of a Higgs boson in the standard-model searches is an encouragement to search for physics beyond the standard model. It is therefore crucial to investigate all topologies that could be of interest to the search for the Higgs boson in the framework of theories beyond the standard one. A substantial effort was undertaken by the LEP experiments to cover not only all possible models but also all possible topologies that could involve Higgs bosons in e^+e^- collisions. In the following section, we report only models for which specific analyses have been designed, along with the salient theoretical predictions that motivate them. (Various models, such as next-to-minimal supersymmetric theories or *CP* violation in the Higgs sector, have also been investigated.)

6.1. Two Higgs Doublets Models (2HDM)

The adjunction of any number of $SU(2)_L$ doublets of complex scalar fields preserves the tree-level relation $\rho = 1$. Here we consider only models with one additional doublet of complex scalar fields, which are the simplest extension of the standard model. In such models, flavor-changing neutral currents can be very large. To avoid this problem, it should be further required that fermions of a given charge do not couple to more than one Higgs doublet. The two most popular models that meet this requirement are the so-called type I models, in which one doublet couples only to fermions and the other to bosons, and the type II models, in which one Higgs doublet couples only to up-type fermions and the other only to down-type fermions. The spontaneous breaking of the electroweak

symmetry, when achieved at the expense of the introduction of two doublets of self-interacting complex scalar fields, leaves five massive scalar physical states that correspond to the remaining five out of eight degrees of freedom available from the two doublets, when the W and Z bosons have absorbed three of them to acquire masses. Among these five Higgs bosons, assuming CP is conserved in the Higgs sector, two are neutral CP-even (h and H, where h denotes the lightest), one is neutral CP-odd (A), and two are charged ($H^{\pm}$). There are six free parameters in this model: the four Higgs boson masses and the mixing angle (α) between the two CP-even Higgs bosons and $\tan\beta$, the ratio of the vacuum expectation values.

6.1.1. TYPE I 2HDMs, FERMIOPHOBIA In the framework of type I 2HDMs, when the CP-even neutral Higgs bosons do not mix, the lightest CP-even Higgs boson does not couple to fermions. When the light boson mass is well below $\sim$100 GeV/c^2, its predominant decay mode is to a pair of photons. Above this threshold, it will also decay to a pair of W bosons of which one is off mass-shell.

In the mass region dominated by the two-photon decay, the search channels are defined by the decays of the accompanying Z boson: $hZ \to \gamma\gamma q\bar{q}$, $hZ \to \gamma\gamma\nu\bar{\nu}$, and $hZ \to \gamma\gamma\ell^+\ell^-$. For all these channels, the major background is the double-radiative Z production. Figure 26 displays the combined result of these searches (46, 47).

For m_h greater than $\sim$100 GeV, where the $h \to WW^*$ branching ratio dominates, L3 performed a dedicated search for topologies with one Z, one W on mass-shell, and one W off mass-shell in the final state (48). This search covered five channels:

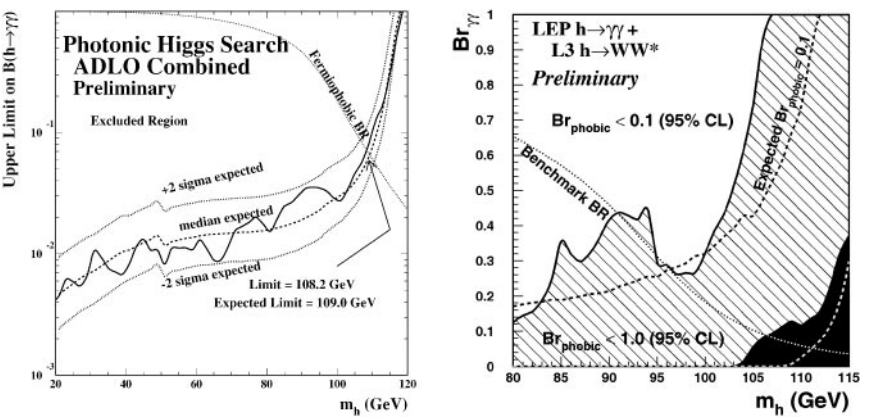

Figure 26 Searches in the context of HDM and fermiophobia: (*a*) Branching ratio limits for $h \to \gamma\gamma$; (*b*) combined limit scan for LEP $h \to \gamma\gamma$ and L3 $h \to WW^*$. Dashed lines show the expected limits; hatched or solid areas show the observed limits. The dark area in the lower right shows the region that is not excluded. The benchmark prediction for BR($h \to \gamma\gamma$) is shown by the dotted line.

$qqqq(qq)$, $qql\nu(qq)$, $qqqq(\nu\nu)$, $qql\nu(\nu\nu)$, and $qqqq(ll)$. The decay mode of the Z is given in parentheses. These five topologies cover a total of 85% of the theoretical branching fraction of $hZ \to WW^* f\bar{f}$ process.

The $h \to \gamma\gamma$ and $h \to WW^*$ search results were combined according to $\mathrm{Br}_{\gamma\gamma}$, which is the fraction of decays to a pair of photons, and $\mathrm{Br}_{\mathrm{phobic}}$, which is the total Higgs branching fraction to pairs of gauge bosons. The values of both m_h and $\mathrm{Br}_{\gamma\gamma}$ are scanned to set a 95% CL exclusion limit on $\mathrm{Br}_{\mathrm{phobic}}$, as shown in Figure 26. The observed limit in the benchmark model is 106.4 GeV and the expected limit is 111.2 GeV (47).

6.1.2. SEARCHES FOR CHARGED HIGGS BOSONS The search for charged Higgs bosons is justified in general 2HDMs. Charged Higgs bosons are produced at LEP in the s-channel via a γ or a Z exchange. In the mass range reachable at LEP (i.e., $m_{H^\pm} < 105$ GeV/c^2), the predominant decay modes are $H^+ \to \tau\nu$ and $H^+ \to c\bar{s}$. The relative contributions of these decay modes mainly depend on the model parameter $\tan\beta$. A limit on the charged Higgs boson mass can be derived only when the three final states corresponding to all combinations of the aforementioned decay modes are investigated, namely $\tau^-\bar{\nu}_\tau\tau^+\nu_\tau$, $\tau^-\bar{\nu}_\tau c\bar{s}$, and $c\bar{s}c\bar{s}$. The topologies arising from these channels are very similar to those originating from a pair of W bosons. The process $e^+e^- \to W^+W^-$ is thus an overwhelming background. The results of the searches in these channels have led to the combined exclusion domain in the plane $(\mathrm{Br}(H^\pm \to \tau\nu), m_{H^\pm})$ shown in Figure 27. The resulting absolute 95% CL lower limit on the charged Higgs boson mass is 78.6 GeV/c^2 in good agreement with the combined sensitivity of 78.8 GeV/c^2. However, in the excluded region of the search, the L3 experiment observed a large excess at a branching fraction of $\sim$0.1. Numerous checks were performed by all experiments to track the origin of this excess. At the time of writing, no definite conclusion had been reached.

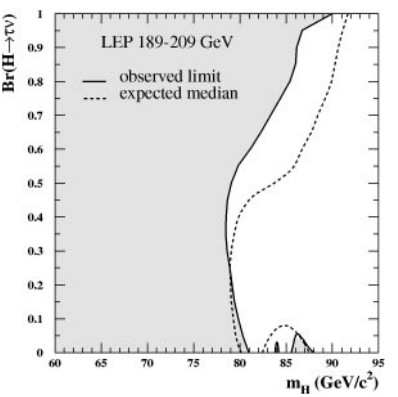

Figure 27 The 95% CL set by LEP experiments (light shaded) and expected (dashed line) exclusion domains in the $(m_h, \mathrm{Br}(H^\pm \to \tau\nu))$ plane.

However, the three other experiments largely excluded any signal hypothesis compatible with the excess observed by L3.

In type I 2HDMs, there is a region in the parameter space of the search, in which additional decay modes should be considered. In these models, when the $H^{\pm} \to W^{\pm}A$ decay is kinematically accessible, it becomes the predominant mode for $\tan\beta > 1$. This exception was studied in detail by the OPAL collaboration (50).

6.1.3. TYPE II 2HDMs, FLAVOR-INDEPENDENT SEARCHES In various extensions of the standard model, particularly in those involving two Higgs doublets, but also in composite models, the coupling of Higgs bosons to b quarks can be suppressed. In the case where the Higgs boson does not predominantly decay to a pair of b quarks, the searches for the standard-model Higgs boson can still be performed, but their sensitivity is greatly reduced because they strongly rely on the tagging of b jets. All four collaborations conducted dedicated searches for the Higgs boson with reduced model dependence, assuming it is produced via the Higgs-strahlung process, and not addressing its flavor of decay. The channels investigated were the same as those used in the search for the standard-model Higgs boson but assumed that the Higgs boson decays into hadrons. These searches are interpreted in terms of a limit on the ratio of the cross section to that in the standard model times the branching fraction of the Higgs boson to hadrons as a function of the Higgs boson mass m_h (51). Assuming that the production rate is that of the standard model and that the Higgs boson exclusively decays to hadrons, a flavor-independent lower limit on the Higgs mass of 112.9 GeV/c^2 is set by combining the data of all four experiments (51).

The OPAL collaboration went further in this direction. It searched for flavor-independent decays of Higgs bosons via associated production, investigating topologies such as four any-quark jets. These searches, combined with both the flavor-independent and the standard search for Higgs bosons, were used in turn to exclude neutral Higgs boson masses in type II 2HDMs (52).

6.2. Minimal Supersymmetry

6.2.1. GENERALITIES Supersymmetry (SUSY) postulates the existence of a bosonic degree of freedom (d.o.f.) for each fermionic d.o.f. and vice versa. The presence of these physical fields provides quadratically divergent corrections to the Higgs boson mass opposite to those due to the standard-model particles. Only logarithmic divergent corrections subsist, but those can be accommodated by the theory. Unlike the standard model (see Section 1.1), supersymmetry is a natural theory. Because the standard model itself is not supersymmetric, a complete spectrum of partner fields is required. The superpartners of fermions are the s-fermions; those of gauge and Higgs bosons are named gauginos and higgsinos, respectively. The neutralinos and charginos are the physical states resulting from the mixing of gauginos and higgsinos in the neutral and charged sector, respectively.

Nevertheless, supersymmetry is broken because the spectrum of superpartner fields has not been observed and the benefits of the theory are gained, in part, at the expense of the introduction of a large number of additional free parameters. A detailed description of supersymmetry can be found in References (55–57).

Contrary to the standard model, a supersymmetric Higgs sector requires at least two Higgs doublets with opposite hypercharge to cancel the higgsino contribution to anomalies. Strong constraints on the Higgs boson masses result from the intimate relationship between the electroweak and SUSY breaking. The minimal supersymmetric standard-model (MSSM) Higgs sector is described entirely by only two free parameters, which are designated m_A and $\tan\beta$. The masses of the Higgs bosons at tree level can then be expressed as follows:

$$m^2_{H^\pm} = m^2_{W^\pm} + m^2_A$$
$$m^2_{h/H} = \frac{1}{2}\left(m^2_A + m^2_Z \mp \sqrt{\left(m^2_A + m^2_Z\right)^2 - 4m^2_Z m^2_A \cos 2\beta}\right).$$

The *CP*-even neutral Higgs boson mixing angle is also fixed by the relation

$$\cos 2\alpha = -\cos 2\beta\left(\frac{m^2_A - m^2_Z}{m^2_H - m^2_h}\right).$$

Simple bounds on the masses of the Higgs bosons can thus be derived at tree level: $m_h < m_Z < m_H$, $m_h < m_A < m_H$ and $m_{H^\pm} > m_{W^\pm}$. Because of the strong coupling of Higgs bosons to the top quark, radiative corrections to m_h from the s-top sector can be very large. The one-loop corrections to the lightest *CP*-even Higgs boson are of the order

$$\frac{3g^2}{8\pi^2}\frac{m^4_t}{m^2_W}\log\left(1 + \frac{m^2_{SUSY}}{m^2_t}\right),$$

where m_{SUSY} is the geometric average of s-top masses. The corrections at the one-loop level (58) have been refined with leading two-loop corrections computed using renormalization group methods (59), renormalization group improvement of the first-order effective potential (60), the two-loop effective potential (61), and the Feynman diagrammatic calculation (62). The mixing in the s-top sector plays a crucial role in these corrections. There are thus three main additional parameters relevant to the Higgs sector that describe the mixing of the s-tops, namely m_{SUSY}, μ (the Higgs mixing parameter), and A_t (the trilinear Higgs-s-top coupling). To interpret experimental results, a specific set of values of all relevant parameters, corresponding to benchmark configurations, are defined (63). The first, called m_h-max, is a configuration of the parameters where m_h is maximized. The second, called no-mixing, corresponds to the case in which the s-tops do not mix and yields an h mass typically close to minimum. The third, called large-μ, corresponds to a case where μ is large relative to m_{SUSY} and a framework where m_h is considerably smaller. With the largest possible correction, m_h is still bounded to be lower than $\sim$130 GeV/c^2. Excluding the mass range up to $\sim$130 GeV/c^2 would

therefore exclude the MSSM. Conversely, a 115 GeV/c^2 Higgs boson would "invite supersymmetry" (65), since at a scale of $\sim 10^6$ GeV, the standard-model potential would become unstable and this instability could be avoided by the presence of s-top bosons and a fine-tuning of the couplings of the model.

6.2.2. PRODUCTION PROCESSES In the MSSM framework, the three production processes described in Section 3.1 are supplemented by the associated production of the lightest *CP*-even Higgs boson (h) and the *CP*-odd Higgs boson (A), $e^+e^- \to Z^* \to hA$. The MSSM cross sections can be expressed relative to the standard-model cross section as follows:

$$\sigma(e^+e^- \to hZ) = \sin^2(\beta - \alpha) \times \sigma_{\rm SM}$$
$$\sigma(e^+e^- \to h\nu_e\bar{\nu}_e, e^+e^-) = \sin^2(\beta - \alpha) \times \sigma(e^+e^- \to H\nu_e\bar{\nu}_e, e^+e^-)_{\rm SM},$$

and for the associated production,

$$\sigma(e^+e^- \to {\rm hA}) = \cos^2(\beta - \alpha) \times \bar{\lambda}\sigma_{\rm SM}.$$

Here, $\sigma_{\rm SM}$ is the standard-model production rate and $\bar{\lambda}$ is a phase-space factor embedding the dependence on m_A of the cross section. The prefactors show that the standard-model–like production processes are complementary to associated production (when one is large, the other is small). The Higgs-strahlung and fusion processes will contribute essentially in the low $\tan\beta$ domain [corresponding to large $\sin^2(\beta - \alpha)$ values], and the associated production will dominate in the high $\tan\beta$ region.

The searches for the standard-model Higgs boson are efficient ways to investigate the low-tan β domain but are inadequate for the high-tan β region. Taking advantage of the associated production is therefore crucial. A reappraisal of the $4b$ and $bb\tau^+\tau^-$ channels from the standard-model search, relaxing the kinematic constraint from the Z, is sufficient to cover the high-tan β domain.

6.2.3. RESULTS To further interpret the hints for the production of an $\sim$115 GeV/c^2 Higgs boson observed in the standard-model searches, it is interesting to first look at the 95% CL exclusion contours within the different MSSM scenarios (illustrated in Figures 28 and 29). The most conservative scenario (m_h-max) in the range $0.5 < \tan\beta < 2.4$ is excluded at the 95% CL (64). If the current interpretation of the experimental data is indeed correct, and the MSSM is nature's choice, the mixing in the s-top sector should be such that the corrections to the Higgs boson mass are large and $\tan\beta$ should be above 2.4. Although large $\tan\beta$ values are not excluded, they are disfavored by the fact that the hints are observed in the standard-model searches.

A combined lower limit of 91.0 GeV/c^2 on the mass of the lightest *CP*-even (h) and of 91.9 GeV/c^2 on the *CP*-odd (A) Higgs bosons of the MSSM can be inferred from these searches. These limits have been further verified beyond the benchmark parameter configurations with a global scan of the MSSM parameter space, which has shown that these limits are robust (31).

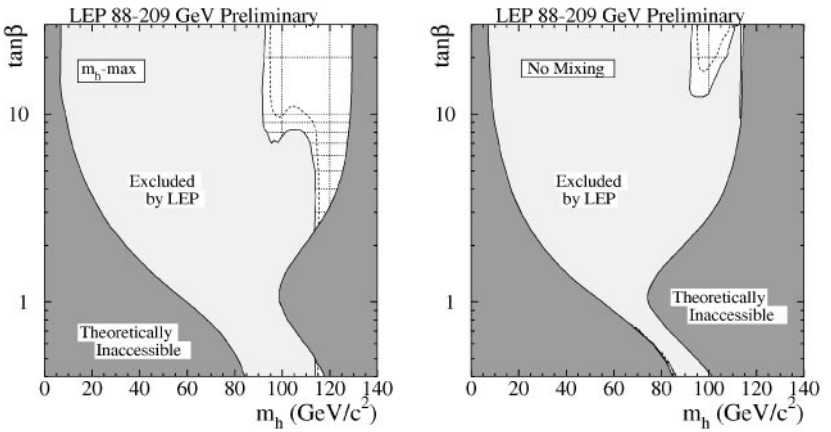

Figure 28 The MSSM 95% CL observed (light shaded) and expected (dashed line) exclusion domains in the (m_h, tan β) plane in the m_h-max (*a*) and no-mixing (*b*) scenarios. The theoretical inaccessible domains are also indicated.

6.3. Beyond the Minimal Symmetric Standard Model

6.3.1. INVISIBLE DECAYS OF THE HIGGS BOSON In an *R*-parity-conserving MSSM, the domains in the model parameter space where the Higgs boson can decay to a pair of neutralinos are typically excluded by direct searches for charginos.

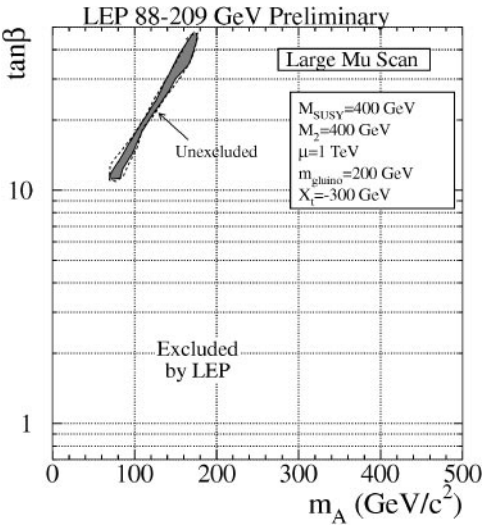

Figure 29 The MSSM 95% CL exclusion domain in the (m_A, tan β) plane in the large-μ scenario.

However, this restriction relies strongly on the assumption that gaugino masses are unified at a large scale. When this assumption is relaxed, there are domains in the MSSM parameter space where the decay of a Higgs boson to the lightest neutralino is allowed (66). Neutralinos are weakly interacting particles and thus escape detection. The Higgs boson decays are thus "invisible." Such decays are also expected in a variety of other models, from theories involving Majorons to large extra dimensions.

To investigate the possibility that a Higgs boson decays invisibly, the topologies with two acoplanar jets and missing energy and two acoplanar leptons and missing energy have been studied, under the assumption that the Higgs boson is produced via the Higgs-strahlung process. The result of these searches established a lower limit on the mass of the Higgs boson as a function of the ratio of its invisible decay rate to that predicted by the standard model (67). The combined lower limit on a Higgs boson, produced at the standard-model rate and decaying exclusively into invisible final states, is 114.4 GeV/c^2.

6.3.2. ANOMALOUS COUPLINGS OF THE HIGGS BOSON The low-energy effects of theories that supersede the standard model at a large scale Λ can be parameterized by an effective Lagrangian. Corrections to the standard-model Lagrangian that alter the couplings of Higgs bosons originate from terms of the type $\mathcal{L}_{\text{eff}} = \sum_n (f_n/\Lambda^2)\mathcal{O}_n$, where the $\mathcal{O}_n$ operator involves both vector and Higgs bosons with couplings f_n. Anomalous couplings of the types $g_{\gamma\gamma}$, $g_{HZ\gamma}$, and g_{HZZ} can arise from the aforementioned operators and affect the expected phenomenology of a standard Higgs sector. For instance, the Higgs boson can be produced in association with a photon and decay in turn to a pair of photons. The DELPHI collaboration searched for topologies with three photons in the framework of anomalous couplings of Higgs bosons (68). No evidence of a signal was observed. This result can be interpreted with the assumption that all f_n relevant for the Higgs anomalous couplings are equal to a generic coupling F. Limits on the generic coupling F can then be set as a function of m_h as shown in Figure 30 (region A).

In this framework, the Higgs boson could also be produced via the Higgs-strahlung process, though still decaying predominantly to photons, and thus give rise to topologies similar to those searched for in the framework of fermiophobia. For the purpose of this combination, only the ALEPH fermiophobic search is reinterpreted in terms of an exclusion of the coupling F as a function of the Higgs boson mass hypothesis. This exclusion is shown in Figure 30 (region C).

The channels described above require nonzero anomalous couplings. Therefore, they cannot explore the small-F region. To further cover this particular domain of the generic coupling F, the searches for the standard-model Higgs boson have been reinterpreted in this more general framework, as shown with ALEPH results in Figure 30 (region B) (31). Combining these interpretations allows setting a lower limit of 106.7 GeV/c^2 on the mass of a Higgs boson that can couple

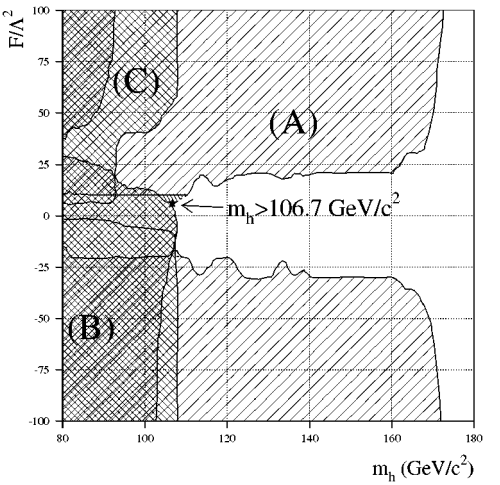

Figure 30 Higgs search beyond the MSSM: 95% CL limits on the generic anomalous coupling F as a function of m_h. Regions A, B, and C are explained in the text.

anomalously to photons with the assumption that all relevant couplings f_n are equal (69).

7. INDIRECT CONSTRAINTS ON THE MASS OF THE HIGGS BOSON

The presence of Higgs field quantum corrections in the electroweak measurements is yet another measure of the self-consistency of the standard-model predictions at low energy. The effect of these quantum corrections can be seen in the following observables: Γ_Z, $A_{FB}^{0,b}$, $A_{FB}^{0,\text{lept}}$, P_τ, m_W, etc., and results in a logarithmic dependence on the Higgs boson mass. The relationship between m_W and m_H as determined from the electroweak data is displayed in Figure 31 and is compared to a recent measurement of the W mass (71). Sensitivity to the Higgs boson mass dependence would not have been possible without the discovery of the top quark and the precise measurement of its mass in addition to the improvements from LEP on the W-mass and $\sin^2\theta_W$ measurements. Current electroweak fit data prefer a value of $\log(m_H) = 1.94 \pm 0.21$, corresponding to a 68% CL interval of [53 GeV/c^2, 141 GeV/c^2] for the Higgs boson mass. In the near future, further improvement of the sensitivity to $\log(m_H)$ is expected from precision measurements of the W and top masses, as well as progress on the hadronic contribution to the running of the electromagnetic coupling constant ($\Delta\alpha^5$). The precision electroweak data have put an unprecedented focus on the discovery of the Higgs boson, or a similar mechanism, in the coming decade.

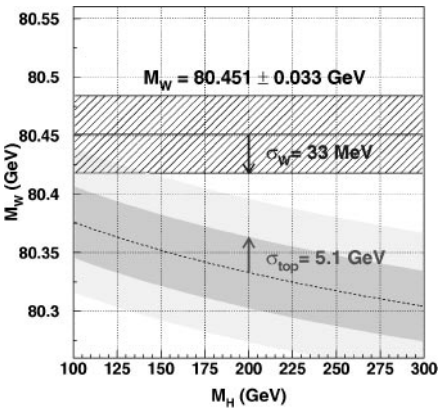

Figure 31 The dotted line is the relationship between m_W and m_H as determined from radiative corrections to the electroweak data. The dominant uncertainty comes from the resolution σ_{top} of the top mass measurement. The solid line represents a recent measurement of the W mass uncertainty.

8. LEGACY AND OUTLOOK

Did LEP observe the first manifestation of the Higgs particle? This exciting question should be answered within the next decade by experiments at present and future hadron colliders. If a Higgs boson with mass close to 115 GeV/c^2 is indeed found, then LEP observed the first hints of its existence. Besides these tantalizing hints, LEP produced a lower limit on the mass of the Higgs boson of 114 GeV/c^2, an unambiguous exclusion of low Higgs boson masses, and pioneering explorations of intricate theoretical models. The stringent limits imposed on the Higgs bosons of the MSSM have motivated a large effort to refine the calculation of two-loop corrections of their masses and have intensified the focus on the remaining available parameters of the theory. Although definitive discovery of the Higgs boson at LEP remained elusive, the standard-model predictions have neither faltered nor waned, bringing both encouragement and uncertainty about what lies ahead.

Further exploration of the direct search will proceed in the immediate future at the Tevatron collider. As with the LEP program, successful gains in sensitivity rely on intense efforts from the accelerator and experimental groups. In particular, since the range of production mechanisms and decay modes is broad, the combined sensitivity of the Tevatron Higgs searches will come from a number of search channels and will depend on the joint contributions from the D0 and CDF collaborations (70). The LEP excess may be a first sign of Higgs production, and a combination of the LEP and Tevatron search data in the 115 GeV/c^2 mass region may resolve this pivotal question in the coming years.

The great expanse opened up by the LHC may show that even the symmetries of $SU(2)_L \otimes U(1)_Y$ are simply relics of a much more profound theory. It is here

that the most decisive and comprehensive investigation of electroweak symmetry breaking will be carried out. A linear e^+e^- collider may be needed to tack down the properties of the Higgs sector in detail. Knowing that broken symmetries and mass are intimately connected through the Higgs mechanism may reveal further ties between elementary particles and fields.

ACKNOWLEDGMENTS

We wish to thank J.-B. de Vivie and R. Zitoun for their careful reading of this report. We are also grateful to Patrick Janot for useful discussions and for sharing his expertise. For MK, this work was supported by the Director, Office of Science, Office of High Energy and Nuclear Physics, of the U.S. Department of Energy under contract no. DE-AC03-76SF00098.

9. APPENDIX: STATISTICAL METHODS

The methods for quantifying and understanding the contributions to the LEP combined Higgs search evolved dramatically from the time of the LEP1 program. Primarily, the experience and competitiveness of the four LEP experiments came together through the activities of the LEP Higgs working group.

The original method for searching came down to a strategy of "cut and count," explicitly removing all background events based on fixed cuts on physical quantities while keeping some efficiency for signal. This method is most effective in background-free searches for new particles. A new approach based on event-by-event discrimination was developed to perform searches in the presence of substantial irreducible backgrounds such as *ZZ* production at LEP2. The *ZZ* production threshold was originally considered to be "the wall" of the LEP2 Higgs search program (28, 2). In a broader perspective, searching for new physics in the presence of backgrounds will be essential to Higgs searches at colliders in the foreseeable future.

Event-by-event discrimination was first developed in the two-variable combination of *b*-tag probability and reconstructed Higgs mass. There are no unique values of this two-variable (x_b, m_H) combination that isolate Higgs production events from the background processes. However, the statistical distribution of (x_b, m_H) provides more physical separation between the presence and absence of Higgs production than simple counting experiments alone.

The discrimination power of the (x_b, m_H) distribution is transformed into near-Gaussian probability density functions for the signal-plus-background and background-only hypotheses according to Section 3.3. The value of Q is the ratio of the likelihood functions for the two hypotheses,

$$Q = L_{s+b}/L_b. \qquad 3.$$

The confidence levels for the two hypotheses, CL_{s+b} and CL_b, for an observed value of Q_{obs} from the data, correspond to the areas of the expected Q distributions

integrating in the signal-like direction for CL_{s+b} and in the background-like direction for CL_b. The expected Q distributions cross at $-2\ln Q = 0$, where the signal-plus-background and the background-only hypotheses are equally probable.

To search for the Higgs boson as a function of mass, m_H, the signal distributions in (x_b, m_H) are simulated in fixed intervals of Higgs mass. The simulated distributions are transformed into continuous functional forms, typically by using the Kernel estimation method (72).[6] These functional forms are interpolated for intermediate Higgs boson masses using various numerical methods (73). The results of scanning in the Higgs boson mass hypothesis are summarized by the values of $-2\ln Q_{\rm obs}$ versus m_H and compared to the median values of the signal-plus-background and background-only hypotheses. Direct estimation of CL_b is aided by adding the 68% and 95% CL intervals on the background-only hypothesis, as shown in Figure 17.

At LEP2 the 95% CL exclusion of the signal hypothesis is set for an observed value of $-2\ln Q_{\rm obs}$ such that $CL_s = CL_{s+b}/CL_b = 5\%$. The quantity CL_s is an approximation for the signal hypothesis that has the relevant property of not allowing the exclusion of signals for large deficits of the observed background rate, i.e., small values of CL_b.

The $-2\ln Q$ statistical estimator is equally sensitive for exclusion and discovery. In the presence of a signal-like excess in the data, it is used to make signal-rate and mass measurements. Figure 19 shows the expected $-2\ln Q_{\rm obs}$ values of the LEP combined Higgs search for a 115.6 GeV/c^2 signal. The best mass estimate is given by the minimum, here corresponding to $m_H = 115.6$ GeV/c^2, and the mass resolution corresponds to the interval [114.5 GeV/c^2, 117 GeV/c^2] given by an increase of $\Delta(-2\ln Q_{\rm obs}) = 1$ above the minimum.[7]

Several methods were developed for checking the consistency of the search analyses. Because $-2\ln Q$ depends on the s/b ratio, the distribution of $\log(s/b)$ gives a clear view of the overall discrimination power of the search, as shown, for example, in Figure 15. The continuity of the assignment of s/b values is checked by the s/b evolution of individual data events, as demonstrated in Figure 25. The comparisons of the relative performances across subchannels and across experiments in rate and mass resolution are crucial for validating the consistency of the background estimations and methods of signal estimation. Variations in search sensitivities are ultimately attributed to analysis optimization and detector performance.

The systematic uncertainties in the background rates and signal efficiencies are compiled by source, as described in Section 5.4.1. Sources that are common to multiple channels and to other experiments are fully correlated. Sources with

[6]To improve the precision of this procedure, either the two-variable distributions are directly convoluted from one-dimensional distributions or the two-dimensional functional forms are forced to reproduce the one-dimensional projections.

[7]The $-2\ln Q$ estimator approaches the $\Delta\chi^2$ distribution in the high-statistics limit where the 68% CL interval corresponds to exactly $\Delta\chi^2 = 1$.

no overlap are treated as uncorrelated. The largest correlated errors within an experiment come from the *b*-tagging information and common uncertainties on background processes.

The quantitative impact of the systematic uncertainties is directly estimated by the range of possible $-2\ln Q$ values for the signal-plus-background and background-only hypotheses. This is determined by keeping the nominal $\ln(1+s/b)$ weights fixed and varying only the mean of the Poisson distributions for the expected signal and background rates with their correlated errors. Keeping the weights fixed gives symmetric treatment for data, signal, and background events while avoiding the artificial reduction of systematic effects that occurs if the weights are simultaneously varied. The error estimates provided channel-by-channel from each of the experiments predict a 68% interval of $-2\ln Q$ values in the range ± 0.45 of the nominal observation. The statistical uncertainty is greater by a factor of 10.

The effect on the observed confidence levels of CL_b and CL_{s+b} from the systematic uncertainties is incorporated via an extension of the method described in Reference (53). Whereas the value of $1-\mathrm{CL}_b$ is 3.2% at $m_H = 115.6$ GeV for statistical errors, it increases to 3.4% when systematic errors are included. The shift in the background confidence level is typically of order 10% toward the median background expectation. The more relevant effect is the range of possible confidence levels predicted from systematic uncertainties. These are obtained by shifting the $-2\ln Q$ values relative to the nominal observation and recomputing the confidence level values. Shifts of ± 0.45 in $-2\ln Q$ correspond to the ranges $1-\mathrm{CL}_b$ [2.4%, 4.4%] and CL_{s+b} [39%, 48%] at $m_H = 115.6$ GeV. The ranges of CL values obtained from this method are substantially larger than the nominal shifts but are still small in comparison to the statistical variation.

LITERATURE CITED

1. Glashow SL. *Nucl. Phys.* 22:579 (1961); Salam A. *Proc. Eighth Nobel Symposium on Elementary Particle Theory, Relativistic Groups, and Analycity*, ed. N Svartholm. Stockholm: Almqvist & Wiksells (1968); Weinberg S. *Phys. Rev. Lett.* 19:1264 (1967)
2. Gunion JF, Haber HE, Kane G, Dawson S. *The Higgs Hunter's Guide*. Reading, MA: Addison Wesley (1990)
3. Higgs PW. *Phys. Lett.* 12:132 (1964). Englert F, Brout R. *Phys. Lett.* 13: 321 (1964); Guralnik GS, Hagen CR, Kibble TW. *Phys. Rev. Lett.* 13:585 (1964)
4. Hambye T, Riesselmann K. *Phys. Rev. D* 55:7255 (1997)
5. SINDRUM Collab. *Phys. Lett.* B 222:533 (1989)
6. Barr GD, et al. *Phys. Lett.* B 235:356 (1990)
7. Sievertz M, et al. (CUSB Collab.). *Phys. Rev. Lett.* 26:717 (1982).
8. Alam MS, et al. (CLEO Collab.). *Phys. Rev. Lett.* 40:712 (1989)
9. Lee-Franzini J, et al. (CUSB Collab.). *Proc.*

Int. Conf. High Energy Phys., XXIVth, Munich, Aug. 4–10, 1988, p. 891. (1989)
10. Aßman R. *Nucl. Phys. B* (*Proc. Suppl*.) In press (2002)
11. Buskulic D, et al. (ALEPH Collab.). *Nucl. Instrum. Methods A* 360:481 (1995)
12. Abreu P, et al. (DELPHI Collab.). *Nucl. Instrum. Methods A* 378:57 (1996)
13. Adeva B, et al. (L3 Collab.). *Nucl. Instrum. Methods A* 289:35 (1989)
14. Adriani O, et al. (L3 Collab.). *Nucl. Instrum. Methods A* 302:53 (1990)
15. Acciarri M, et al. (L3 Collab.). *Nucl. Instrum. Methods A* 351:300 (1994)
16. Ahmet K, et al. (OPAL Collab.). *Nucl. Instrum. Methods A* 305:275 (1991)
17. Allport PP, et al. (OPAL Collab.). *Nucl. Instrum. Methods A* 346:476 (1994)
18. Anderson S, et al. (OPAL Collab.). *Nucl. Instrum. Methods A* 403:326 (1997)
19. Bjorken JD. *Proc. SLAC Summer Institute, Stanford*, ed. M Zipf (1977)
20. Wilczek F. *Phys. Rev. Lett.* 39:1304 (1977)
21. Janot P. LAL 89–45 (1989)
22. Decamp D, et al. (ALEPH Collab.). *Phys. Lett.* B 236:233 (1990)
23. Janot P. In *Perspectives in Higgs Physics*, ed. GL Kane, 17:104 (1997)
24. Buskulic D, et al. (ALEPH Collab.). *Phys. Lett.* B 384:427 (1996)
25. Abreu P, et al. (DELPHI Collab.). *Phys. Lett.* B 421:3 (1994)
26. Acciarri M, et al. (L3 Collab.). *Phys. Lett.* B 385:454 (1996)
27. Alexander G, et al. (OPAL Collab.). *Z. Phys. C* 73:189 (1997)
28. Carena M, et al. In *Physics at LEP2*, ed. G Altarelli, T Sjöstrand, F Zwirner, 1:351. CERN 96-01 (1996)
29. Janot P. In *Physics at LEP2*, ed. G Altarelli, T Sjöstrand, F Zwirner, 2:309. CERN 96-01 (1996)
30. Kilian W, Kramer M, Zerwas PM. *Phys. Lett.* B 373:135 (1996)
31. Barate R, et al. (ALEPH Collab.). *Phys. Lett.* B 499:53 (2001)
32. Abdallah J, et al. (DELPHI Collab.). *Eur. Phys. J. C* 23:909 (2002)
33. Acciarri M, et al. (L3 Collab.). *Phys. Lett.* B 508:225 (2001)
34. The LEP Higgs Working Group. CERN-EP/2000-055
35. Janot P. *Proc. Xth Chamonix Workshop* (2000). http://cern.web.cern.ch/CERN/Divisions/SL/publications/
36. Myers S, Wyss C. In *Physics at LEP2*, ed. G Altarelli, T Sjöstrand, F Zwirner, 1:23. CERN 96–01 (1996)
37. Treille D. *Nucl. Phys. B* (*Proc. Suppl*.) In press (2002)
38. Tully C. LEPC seminar, CERN, Sept. 5 (2000)
39. The LEP Higgs Working Group, LHWG note 2001–03, contributed to EPS 2001 and LP'01
40. Barate R, et al. (ALEPH Collab.). *Phys. Lett.* B 495:1 (2000)
41. Heister A, et al. (ALEPH Collab.). *Phys. Lett.* B 526:191 (2002)
42. Abreu P, et al. (DELPHI Collab.). *Phys. Lett.* B 499:23 (2001)
43. Acciarri M, et al. (L3 Collab.). *Phys. Lett.* B 495:18 (2000)
44. Achard P, et al. (L3 Collab.). *Phys. Lett.* B 517:319 (2001)
45. Abbiendi G, et al. (OPAL Collab.). *Phys. Lett.* B 499:38(2001)
46. The LEP Higgs Working Group, LHWG note 2001–08, contributed to EPS 2001 and LP'01
47. Mans J. *Proc. Seventh Topical Seminar on the Legacy of LEP and SLC, 2001*
48. L3 Collab. L3 Note 2685. Contributed to ICHEP 2001
49. The LEP Higgs Working Group, LHWG Note 2001–05, contributed to EPS 2001 and LP'01
50. OPAL Collab. Physics Note PN472 (2001)
51. The LEP Higgs Working Group, LHWG note 2001–07, contributed to EPS 2001 and LP'01
52. OPAL Collab. Physics Note PN475 (2001)
53. Cousins RD, Highland VL. *Nucl. Instrum. Methods A* 320:331 (1992)
54. Helene O. *Nucl. Instrum. Methods A* 212: 319 (1983)

55. Drees M. hep-ph/9611409
56. Nilles HP. *Phys. Rep.* 110:1 (1984)
57. Martin SP. In *Perspectives on Supersymmetry*, ed. GL Kane, pp. 1–98. Singapore: World Sci. (1997)
58. Barbieri R, Frigeni M. *Phys. Lett.* B 258: 395 (1991)
59. Carena M, Quirós M, Wagner CEM. *Phys. Lett.* B 461:405 (1996)
60. Ellis J, Ridolfi G, Zwirner F. *Phys. Lett.* B 262:477 (1991)
61. Hempfling R, Hoang A. *Phys. Lett.* B 331: 99 (1994); Zhang R-J. *Phys. Lett.* B 447:89 (1999)
62. Heinemeyer S, Hollik W, Weiglein G. *Phys. Lett.* B 440:296 (1998); Heinemeyer S, Hollik W, Weiglein G. *Eur. Phys. J. C* 9:343 (1999)
63. Carena M, Heinemeyer S, Wagner CEM, Weiglein G. CERN-TH/99-374
64. The LEP Higgs Working Group. LHWG Note 2001-04, contributed to EPS 2001 and LP'01
65. Ellis J, Ross D. *Phys. Lett.* B 506:331 (2001)
66. Djouadi A, Janot P, Kalinowski J, Zerwas PM. *Phys. Lett.* B 376:220 (1996)
67. The LEP Higgs Working Group. LHWG Note 2001-06, contributed to EPS 2001 and LP'01
68. DELPHI Collab. Note 2000-033, CONF 352
69. Kado M. In *Proc. XXXVth Rencontres de Moriond*, hep-ex/0005022
70. Carena M, et. al. FERMILAB-CONF/00-279-T, SCIP-00-37 (2000)
71. LEP and SLD Electroweak Working Group. CERN-EP/2001-098
72. Cranmer KS. *Comp. Phys. Comm.* 136:198 (2001)
73. Read AL. *Nucl. Instrum. Methods A* 425: 357 (1999)

Annual Review of Nuclear and Particle Science
Volume 52, 2002

CONTENTS

FRONTISPIECE, *Milla Baldo Ceolin* xii

THE DISCREET CHARM OF THE NUCLEAR EMULSION ERA, *Milla Baldo Ceolin* 1

PION-NUCLEUS INTERACTIONS, *T.-S. H. Lee and R. P. Redwine* 23

THE SEARCHES FOR HIGGS BOSONS AT LEP, *M. M. Kado and C. G. Tully* 65

DOUBLE BETA DECAY, *Steven R. Elliott and Petr Vogel* 115

FLUX OF ATMOSPHERIC NEUTRINOS, *T. K. Gaisser and M. Honda* 153

THE MASS OF THE *b* QUARK, *Aida X. El-Khadra and Michael Luke* 201

PHYSICS OPPORTUNITIES AT NEUTRINO FACTORIES, *J. J. Gomez-Cadenas and D. A. Harris* 253

MOLECULAR IMAGING WITH POSITRON EMISSION TOMOGRAPHY, *Michael E. Phelps* 303

EFFECTIVE FIELD THEORY FOR FEW-NUCLEON SYSTEMS, *Paulo F. Bedaque and Ubirajara van Kolck* 339

PARTICLE PHYSICS PROBES OF EXTRA SPACETIME DIMENSIONS, *JoAnne Hewett and Maria Spiropulu* 397

THE RHIC ACCELERATOR, *M. Harrison, S. Peggs, and T. Roser* 425

INDEXES

Cumulative Index of Contributing Authors, Volumes 43–52 471

Cumulative Index of Chapter Titles, Volumes 43–52 474

ERRATA

An online log of corrections to *Annual Review of Nuclear and Particle Science* chapters may be found at http://nucl.annualreviews.org/errata.shtml